energies

MDPI

*Article*

# Derivation of Equivalent Soil Thermal Resistivity for EHVDC Cable Design in Layered Offshore Seabed Conditions

**Francesco Mattioli [1], Ioannis Chatzis [2], Lukasz Chmura [2], Beate Simon [2], Frank de Vries [2] and Mohamad Ghaffarian Niasar [1,*]**

[1] Department of Electrical Sustainable Energy, Faculty of Electrical Engineering, Mathematics and Computer Science, Delft University of Technology, Mekelweg 4, 2628 CD Delft, The Netherlands; francesco.mattiolimn@gmail.com
[2] TenneT TSO B.V., Utrechtseweg 310, 6812 AR Arnhem, The Netherlands
* Correspondence: m.ghaffarianniasar@tudelft.nl

**Abstract**

Accurate assessment of soil thermal resistivity is important for the reliable thermal design of buried EHVDC cable systems, especially along offshore routes where seabed conditions are variable and only measured at discrete locations. This paper develops a methodology to derive an equivalent soil thermal resistivity from layered offshore soil profiles for use in standard ampacity calculations and the tendering process. The method combines geotechnical interpretation, statistical characterisation of soil types, and a conformal-mapping-based thermal solver. The methodology is validated against finite-element simulations, showing good agreement, and is further evaluated through sensitivity studies on far-field soil conditions and spatial variability around the cable. The results indicate that far-field soil assumptions and small lateral variations have only a limited effect on the equivalent thermal resistivity, while greater uncertainty arises when high-resistivity layers, layer continuity, or missing measurements affect the soil conditions near the cable depth. The proposed framework provides transmission system operators with a transparent and reproducible basis for interpreting soil thermal data, supporting robust cable design, tender comparability, and offshore route assessment.

**Keywords:** thermal resistivity; equivalent thermal resistivity; soil; conformal mapping; EHVDC cables; HVDC cables; ampacity; offshore energy; submarine power cables; cable routing

Check for updates

Academic Editors: Yihan Xing, Fengmei Jing and Renwei Ji

Received: 7 October 2026
Revised: 26 October 2026
Accepted: 28 October 2026
Published: 30 October 2026

**Copyright:** © 2026 by the authors. Licensee MDPI, Basel, Switzerland. This article is an open access article distributed under the terms and conditions of the Creative Commons Attribution (CC BY) license.

## 1. Introduction

Recent developments in renewable energy have been significant in the North Sea region. The total installed offshore wind generation capacity planned for this area is expected to exceed 100 GW by 2050 [1,2]. This development requires offshore wind farms to be located farther from shore, resulting in offshore-to-onshore transmission connections that can exceed 100 km in length. Consequently, submarine power cables are increasingly being installed in areas where the seabed conditions are not yet well characterised. Once a preferred cable route has been selected, the seabed stratigraphy and its thermal properties must be investigated. However, practical and economic limitations prevent detailed soil investigations from being performed continuously along the entire route. Typically, seabed soil samples are collected at intervals of approximately 1 km and from depths of up to 6 m below the seabed surface. The resulting measurements therefore provide only discrete information about the soil conditions along the cable route. The interpreted soil

layers, together with their measured or assigned thermal resistivity values, can be used to assess cable thermal performance and ampacity. The aim of this study is to develop and validate a reproducible methodology for converting discrete offshore geotechnical and thermal resistivity measurements into continuous layered soil profiles and, subsequently, into equivalent homogeneous thermal resistivity values suitable for standard cable ampacity calculations. This approach allows the thermal influence of layered seabed conditions to be incorporated into standard ampacity calculations and supports the selection of a cable design suitable for the required power transmission capacity. This study also assesses how uncertainties in soil characterisation, far-field conditions, lateral variability, and burial depth influence the calculated equivalent thermal resistivity. Several studies have investigated the thermal behaviour and ampacity of buried HVDC submarine cables using analytical or finite-element methods. These studies have considered factors such as burial depth, cable configuration, environmental conditions, and the thermal properties of the surrounding soil [3–5]. However, they generally assume that the required soil thermal properties are already known and representative of the soil domain relevant to the calculation. In parallel, previous publications and industry guidance have described offshore geotechnical investigation methods and laboratory and in situ measurements of soil thermal resistivity [6,7]. Nevertheless, limited attention has been given to the complete procedure required to convert discrete offshore investigation data into continuous layered thermal resistivity profiles suitable for cable-rating calculations. In particular, the representativeness of individual measurements, their assignment to interpreted soil layers, and the adequacy of the investigated soil volume surrounding the cable have not been comprehensively addressed. The conformal-mapping formulation adopted in this study follows the approach described in [8]. The novelty of the present work lies not in the underlying formulation itself, but in its integration into a complete workflow that addresses the interpretation of sparse offshore measurements, the assignment of thermal resistivity to unmeasured layers, and the spatial uncertainty associated with the investigated soil profile. The resulting methodology is validated against finite-element simulations and applied to actual soil profiles along an offshore HVDC cable route.

## 2. Input Parameters for Ampacity Calculations

TenneT, as the Dutch transmission system operator, develops offshore grid connections to integrate offshore wind energy into the onshore network using extra-high-voltage direct-current cable systems. During the conceptual design phase of a DC transmission link, stakeholder consultations are carried out with authorities and regulatory bodies to address permitting, environmental, and spatial constraints. These activities lead to the selection of a preferred cable route.

Subsequently, TenneT launches tenders inviting cable suppliers to design, manufacture, and install the cable system. Acting as the employer, TenneT defines the technical and performance requirements through its Employer Requirements. These requirements ensure that the cable system is fit for purpose and capable of reliably transmitting the required power along the selected route throughout its operational lifetime.

Following contract award, during the cable design phase, manufacturers develop EHVDC cable systems in compliance with TenneT's Employer Requirements, international standards, and relevant CIGRé guidelines, such as IEC 60287 and CIGRé Technical Brochure 852 [9,10]. The cable design, validated through a qualification regime including type and prequalification tests, must ensure that thermal and electrical limits are respected under operating conditions.

A key objective of the design is to ensure that the cable can continuously transmit the required current while maintaining the conductor temperature below the specified

maximum limit, $T_{cond,max}$. For DC XLPE insulation, this limit is typically 70 °C and is verified through qualification testing. The conductor temperature is primarily driven by ohmic losses, $I^2R$, which depend on the conductor material and cross-sectional area. Exceeding the specified conductor temperature limit accelerates insulation ageing and increases the risk of failure; therefore, this limit defines the upper boundary for ampacity.

For EHVDC cables, another critical constraint for ampacity is the temperature gradient across the insulation system [11]. Both maximum and minimum limits of the temperature difference, $\Delta T$, are defined and verified during qualification testing. The maximum temperature difference, $\Delta T_{max}$, represents the allowable thermal stress across the insulation, while the minimum value, $\Delta T_{min}$, ensures sufficient outward heat flux to avoid thermal instability. In design terms, this requires that, at $T_{cond,max}$, the temperature at the outer semiconductive layer remains below $T_{cond,max} - \Delta T_{min}$, preventing localised overheating of the insulation.

The relationship between current rating and temperature is described analytically in the IEC 60287 series [9], which provides thermal balance equations linking conductor temperature to losses, cable construction, and thermal resistances. Ampacity is therefore a function of the allowable conductor temperature, the internal thermal resistances of the cable layers, the installation configuration, such as burial depth, spacing, or bundling, and the external thermal environment.

A key parameter in this framework is $T_4$, which represents the external thermal resistance between the cable surface and the surrounding medium. This parameter captures the influence of the installation environment and is strongly dependent on soil thermal resistivity, $\rho$, and ambient temperature. For buried cables, soil conditions are a dominant factor. Materials such as sand generally exhibit relatively low thermal resistivity, enabling efficient heat dissipation, whereas clay or peat may reach significantly higher values, thereby limiting cooling capability.

Consequently, while cable geometry and materials define the internal thermal performance, the external thermal resistance, $T_4$, often governs the final current rating. Accurate characterisation of this parameter is therefore essential to ensure a fit-for-purpose design and to avoid adverse conditions such as thermal runaway, where generated heat exceeds the ability of the surrounding environment to dissipate it.

To accurately quantify the external thermal environment represented by $T_4$, dedicated offshore survey campaigns are carried out along the selected cable route. These campaigns typically combine geophysical and geotechnical investigations to characterise seabed conditions, including soil layering, material composition, and burial feasibility. A key outcome is the determination of soil thermal resistivity, which directly governs heat dissipation from the cable into the surrounding medium.

From a thermal design perspective, the most relevant parameters derived from the survey campaigns are soil thermal resistivity, ambient temperature, and depth of burial. Together, these define the boundary conditions for ampacity calculations and feed directly into the determination of $T_4$ according to IEC 60287 [9].

## 3. Derivation of the Equivalent Soil Thermal Resistivity

As discussed in the previous section, the thermal resistivity of the surrounding soil strongly influences heat dissipation and therefore affects the cable design required for the ampacity specified by TenneT. High soil thermal resistivity limits heat transfer from the cable to the surrounding environment, resulting in higher cable temperatures and potentially more conservative design choices, such as larger conductor cross-sections or materials with higher electrical conductivity. In contrast, low soil thermal resistivity improves cooling and may allow for more optimised and cost-effective cable designs.

Ampacity calculations can be performed using either standard analytical methods or numerical finite-element tools. The analytical method commonly used for steady-state cable rating is based on the IEC 60287 series, where the cable system is represented by a network of thermal resistances and the current rating is calculated from the balance between heat generation and heat dissipation [9,12]. This approach is fast, transparent, and well suited for routine calculations and design checks. However, the analytical formulation generally requires the surrounding soil to be represented as a homogeneous medium with a single thermal resistivity value.

In reality, offshore seabed soils are often heterogeneous and may consist of several layers with different thermal properties. Finite-element tools, such as COMSOL Multiphysics® version 6.3, can represent these layered soil profiles more explicitly by assigning individual geometries and thermal resistivity values to each layer. This makes FEM useful for detailed design verification and for studying complex configurations. However, FEM is less practical for systematic route-wide assessment because each investigation location and burial depth requires geometry definition, material assignment, meshing, and post-processing.

For this reason, an equivalent soil thermal resistivity is derived to act as a bridge between detailed layered soil data and standard ampacity calculation tools. In this study, the equivalent thermal resistivity is defined as the thermal resistivity of a homogeneous soil that produces the same thermal response as the interpreted layered seabed profile for a given investigation location and cable burial depth. It is therefore not a simple average of the measured values, but a calculated engineering parameter representing the combined thermal effect of the surrounding soil layers.

The equivalent thermal resistivity is determined separately for each investigation location. It depends on the local soil stratigraphy, the thermal resistivity values assigned to each layer, and the selected cable burial depth, which is defined by TenneT TSO BV as part of the project design basis. Since heat transfer is mainly governed by the soil conditions in the vicinity of the cable, different burial depths may result in different equivalent thermal resistivity values for the same layered soil profile.

Besides making the layered soil information compatible with standard ampacity calculations, the equivalent thermal resistivity also provides a common design input for the tendering process. The derivation of this parameter directly affects the cable design required for a given ampacity, because different assumptions regarding soil layering, missing measurements, layer averaging, burial depth, or conservative interpretation may lead to different calculated cable temperatures.

The interpretation of the soil data is therefore partly subjective. Thus, if it were left entirely to the cable manufacturers, each bidder could apply different assumptions and calculation conditions. The submitted designs would therefore not be based on the same design basis, making a fair technical comparison difficult. Since TenneT TSO BV operates as a public entity, the tendering process must remain transparent, reproducible, and comparable between manufacturers. A consistent procedure for deriving the equivalent thermal resistivity reduces the amount of interpretation left to individual manufacturers and ensures that all parties use the same soil thermal input.

The derivation procedure consists of four main steps: investigation of seabed conditions along the cable route, laboratory testing of recovered soil samples, development of layered thermal resistivity profiles, and conversion of these profiles into equivalent homogeneous thermal resistivity values for the selected burial depth. The following sections describe these steps in more detail.

### *3.1. Soil Investigation and Thermal Resistivity Measurements*

The derivation of an equivalent soil thermal resistivity requires a simplified but representative description of the seabed surrounding the cable, including both the vertical soil layering and the thermal resistivity assigned to each layer. For this purpose, the dataset considered in this study comprises 198 investigation locations distributed across the three cable routes shown in Figure 1. This subsection describes the available geotechnical and thermal resistivity data and explains how these data are combined to construct layered thermal resistivity profiles.

This study is based on offshore cable route areas of interest for TenneT TSO BV. The available data include Cone Penetration Test results, vibrocore descriptions, laboratory classification tests, and thermal resistivity measurements. The routes are located relatively close to each other, which makes it possible to compare several soil datasets within a limited geographical area.




**Figure 1.** Overview of the TenneT cable routes considered in this study, prepared by the authors based on project data. The different colors distinguish the considered cable routes, while the green markers indicate their endpoints.

The geotechnical characterisation of the seabed is primarily based on two investigation techniques: Cone Penetration Testing (CPT/CPTU) and vibrocore sampling. Together, these methods provide the stratigraphic framework and physical soil samples required to develop the layered thermal resistivity profiles used in this study. During a CPT, a cone attached to a series of rods is pushed into the ground at a constant rate while sensors continuously measure cone resistance $q_c$ and sleeve friction $f_s$ [13]. A schematic representation of the cone penetrometer and its principal measurement components is shown in Figure 2. These parameters are used to characterise the soil type encountered, identify changes in soil behaviour, and define layer boundaries with depth. Although CPT/CPTU tests do not directly provide thermal properties, they provide the stratigraphic framework needed to assign measured thermal resistivity values to the corresponding soil layers.

Vibrocore sampling complements the CPT/CPTU data by recovering physical soil samples from selected depths. The recovered samples allow the interpreted soil layers to be visually described and classified while also providing specimens for laboratory thermal testing. By correlating the vibrocore descriptions with the CPT/CPTU results, the mea-

sured thermal properties can be assigned to the appropriate stratigraphic units along the investigated route.

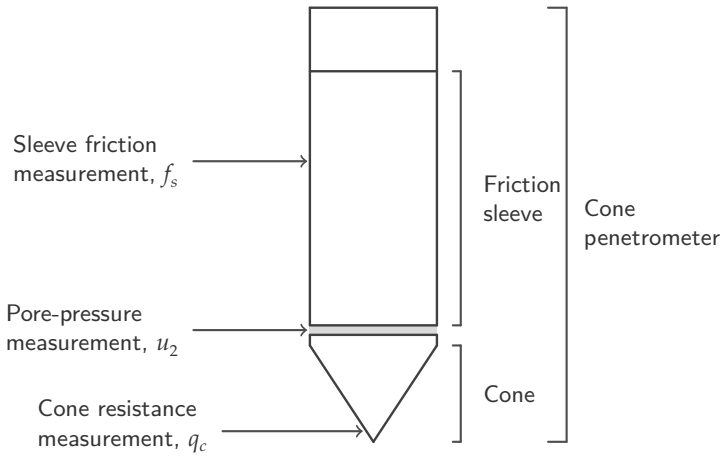


**Figure 2.** Schematic representation of a cone penetrometer used in CPT/CPTU investigations, adapted from [14].

Thermal resistivity is primarily measured on recovered vibrocore samples using a transient needle-probe method. A probe containing a heating element and a temperature sensor is inserted into the soil specimen. Once thermal equilibrium has been reached, a controlled heat input is applied, and the resulting temperature response is recorded.

Thermal conductivity is determined from the relationship between temperature and logarithmic time, while thermal resistivity is calculated as its reciprocal [15,16].

This laboratory method provides controlled measurements and enables the resulting thermal properties to be linked to the soil layers identified through CPT/CPTU interpretation and vibrocore descriptions. However, the measured values may be affected by specimen disturbance, moisture redistribution, compaction, test temperature, salinity, and stress relief following sample recovery.

To assess the representativeness of the laboratory measurements, in situ thermal resistivity measurements were also performed at selected locations along the cable route. These measurements apply the same transient heat-impulse principle directly within the seabed, thereby preserving the natural soil structure and moisture conditions more effectively. The measurement concept involves inserting a heated probe into the seabed, recording the temperature response during heating and cooling, and interpreting the resulting data using line-source heat-transfer theory [15,17].

The comparison confirmed differences between the two methods. Laboratory values were generally higher than the corresponding in situ values, with differences of up to approximately 30% for some sandy soils, while much smaller differences, up to 5%, were observed for clayey soils. However, only a limited number of paired measurements were available, which was insufficient to establish a reliable correction factor. These observations are therefore project-specific and should not be generalised.

In situ measurements are generally more representative of natural seabed conditions, but they require dedicated offshore operations and are therefore more costly and time-consuming than laboratory measurements. For this reason, they are typically performed only at selected locations. Although laboratory measurements may not provide exact in situ thermal resistivity values, they remain sufficiently representative to identify high-thermal resistivity layers and unfavourable soil conditions along the cable route.

Since not every interpreted soil layer contains a direct thermal resistivity measurement, additional support is required to assign representative values in a consistent way. Therefore,

before constructing the final layered thermal resistivity profiles, a statistical analysis of the available measurements is performed. This analysis provides typical thermal resistivity values for the main soil types encountered along the cable route and supports the treatment of layers where direct measurements are missing.

### *3.2. Statistical Analysis of Thermal Resistivity Measurements*

The measured thermal resistivity values were grouped according to the main soil types encountered along the TenneT cable-route corridor. For each soil type, several candidate probability distributions were fitted to the data, including normal, lognormal, Weibull, gamma, and Rayleigh distributions. The distribution parameters were estimated using maximum likelihood estimation, while the goodness of fit was evaluated using the Akaike Information Criterion and the Bayesian Information Criterion [18,19]. An example of the lognormal distribution fitted to the measured thermal resistivity values for sand is shown in Figure 3.

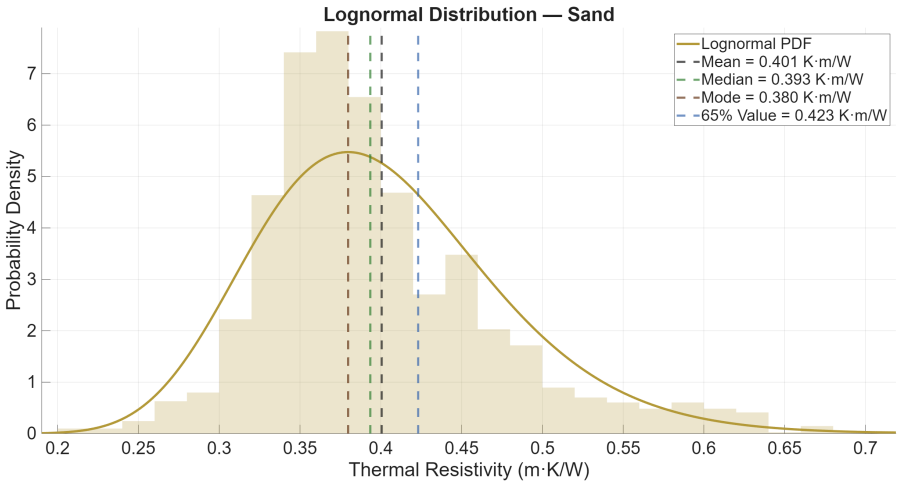


**Figure 3.** Example of a lognormal distribution fitted to measured thermal resistivity values for sand.

Among the candidate distributions, the lognormal distribution provided the best fit for the main soil types analysed. It was therefore selected as the statistical model for deriving representative soil-type-specific thermal resistivity values. For each soil type, the representative thermal resistivity assigned to an interpreted layer without a direct measurement was generally taken as the 65th percentile of the fitted lognormal distribution. This percentile was selected to provide a moderately conservative estimate while remaining representative of the measured soil-type-specific distribution. Where measurements of the same soil type were available in the surrounding investigation area, the assigned value could be adapted through engineering interpretation of these local measurements to better represent the site-specific soil conditions. Any such adaptation was therefore constrained by measured values from geotechnically comparable soils within the investigated cable-route corridor. This procedure provides a consistent and reproducible basis for assigning thermal resistivity values to interpreted soil layers for which no direct measurement is available.

### *3.3. Development of Layered Thermal Resistivity Profiles*

For each investigation location, a layered thermal resistivity profile was constructed by combining the continuous stratigraphic interpretation derived from CPT/CPTU data and vibrocore descriptions with the available thermal resistivity measurements and the representative soil-type-specific values derived in Section 3.2. Different assignment rules were applied depending on the availability and distribution of the measurements. When a direct thermal resistivity measurement was available within an interpreted soil layer, the

measured value was assigned to the corresponding interval. If multiple measurements occurred within the same layer, the layer was not represented by a single average value. Instead, where supported by the visual core description and CPT/CPTU interpretation, it was subdivided into smaller intervals. This approach preserves vertical variability and avoids excessive smoothing of the thermal resistivity profile. When an interpreted soil layer contained no direct measurement, a representative value derived from the statistical analysis was assigned according to the corresponding soil type. This approach ensures that unmeasured intervals are treated consistently while remaining linked to the interpreted soil classification and the range of thermal resistivity values measured along the cable route. Below the investigated depth, where direct measurements and detailed stratigraphic information were unavailable, the soil was assigned a constant thermal resistivity based on the dominant soil type or a representative value from the available dataset. This assumption provides a complete thermal resistivity profile over the full depth of the numerical domain. The resulting layered profiles were subsequently used to calculate the equivalent homogeneous thermal resistivity required for standard ampacity calculations.

## 4. Conformal-Mapping-Based Calculation Tool

The layered thermal resistivity profiles developed in Section 3.3 are converted into equivalent homogeneous values using a conformal-mapping-based calculation tool. The tool evaluates the thermal response of a buried cable within the layered soil profile and determines the thermal resistivity of a homogeneous soil that produces the same cable temperature. The resulting equivalent thermal resistivity therefore represents the combined thermal effect of the layered seabed while remaining compatible with standard ampacity calculations.

In this study, this conversion is performed using a conformal-mapping-based calculation tool. The purpose of the tool is to evaluate the thermal response of a buried cable in a multilayer soil profile and to determine the homogeneous soil thermal resistivity that produces the same cable temperature. In this way, the equivalent thermal resistivity retains the main thermal effect of the layered seabed while remaining compatible with standard cable rating calculations.

Conformal mapping is used to transform the physical cable–soil domain into a rectangular computational domain. This transformation simplifies the geometry of a circular buried cable below a flat seabed surface and allows the soil layers to be discretised in a structured way. The thermal resistivity assigned to each mapped region corresponds to the value assigned to the original soil layer in the physical domain. As a result, the layered nature of the seabed is preserved in the calculation, while the mathematical problem becomes easier to solve.

### *4.1. Conformal Mapping of the Cable–Soil Domain*

The conformal mapping used in this study follows the approach described in the ELECTRA 98 report [8]. Its purpose is to transform the physical cable–soil geometry into a rectangular computational domain. This makes the original geometry, consisting of a circular buried cable below a flat seabed surface, easier to discretise and solve numerically. The transformation used to obtain this mapped domain is defined as follows:

$$w = \Phi(z) = \ln\left(\frac{z + jy_1}{z - jy_1}\right), \tag{1}$$

where $z = x + jy$ is the coordinate in the physical plane and $w = u + jv$ is the coordinate in the transformed plane. The parameter $y_1$ is defined as follows:

$$y_1 = \sqrt{L'^2 - \left(\frac{D_e}{2}\right)^2}, \tag{2}$$

where $L'$ is the vertical distance from the seabed surface to the cable centreline, and $D_e$ is the external cable diameter. In engineering practice, as well as in this study, the burial depth $L$ is measured from the seabed surface to the top of the cable. The centreline depth required by the conformal-mapping model is therefore:

$$L' = L + \frac{D_e}{2}. \tag{3}$$

All burial depths were converted to centreline depth before being used in the conformal-mapping calculations.

This choice of $y_1$ ensures that the circular cable surface in the physical domain is transformed into a straight boundary in the transformed domain. More specifically, the cable surface is mapped to:

$$u = -u_e, \tag{4}$$

where

$$u_e = \ln\left(\frac{2L' + \sqrt{4L'^2 - D_e^2}}{D_e}\right). \tag{5}$$

The seabed surface, corresponding to $y = 0$ in the physical domain, is mapped to $u = 0$, while the second coordinate $v$ is periodic with the total range $v_e = 2\pi$.

Thus, the infinite physical cable–soil domain is represented by the finite rectangular domain:

$$-u_e \le u \le 0, \qquad 0 \le v < 2\pi. \tag{6}$$

In this domain, $u = -u_e$ represents the cable surface and $u = 0$ represents the seabed surface. The boundaries $v = 0$ and $v = 2\pi$ are periodic and represent the two mapped sides of the same physical line.

### *4.2. Transformation of a Multilayer Soil Profile*

After the cable–soil geometry has been transformed into the rectangular $u$-$v$ domain, the same conformal mapping is applied to the boundaries of the interpreted soil layers. In the physical domain, shown in Figure 4, the seabed profile is represented by horizontal layers, each defined by its depth interval and assigned thermal resistivity. The red line in the figure indicates the branch cut of the logarithmic mapping, which is mapped onto the periodic lateral boundaries of the transformed domain.

When the conformal transformation is applied, the horizontal layer boundaries in the physical domain are no longer horizontal in the mapped domain. Instead, they become curved boundaries that divide the rectangular $u$-$v$ domain into different soil regions, as shown in Figure 5. Each transformed region corresponds to one layer, or sub-layer, of the original stratigraphy.

The thermal resistivity assigned to a region in the transformed domain is the same as the thermal resistivity assigned to the corresponding soil layer in the physical domain. In this way, the non-homogeneous soil profile is preserved in the mapped domain, while the external cable–soil geometry remains represented by a rectangular computational domain.

The explicitly defined stratigraphy is limited to the depth covered by the soil investigation, typically 5–6 m below the seabed. Below the lowest identified layer, the deeper soil is represented as a homogeneous far-field region. Similarly, in the horizontal direction, the interpreted layers are assigned a finite lateral extent, while the soil outside this region is treated as homogeneous. These far-field regions are included because the conformal

mapping represents an infinite physical domain within a finite mapped domain. Their influence on the equivalent thermal response is expected to be limited, since heat transfer is mainly governed by the soil located close to the cable. This assumption is examined in the sensitivity analysis presented in Section 5.4.

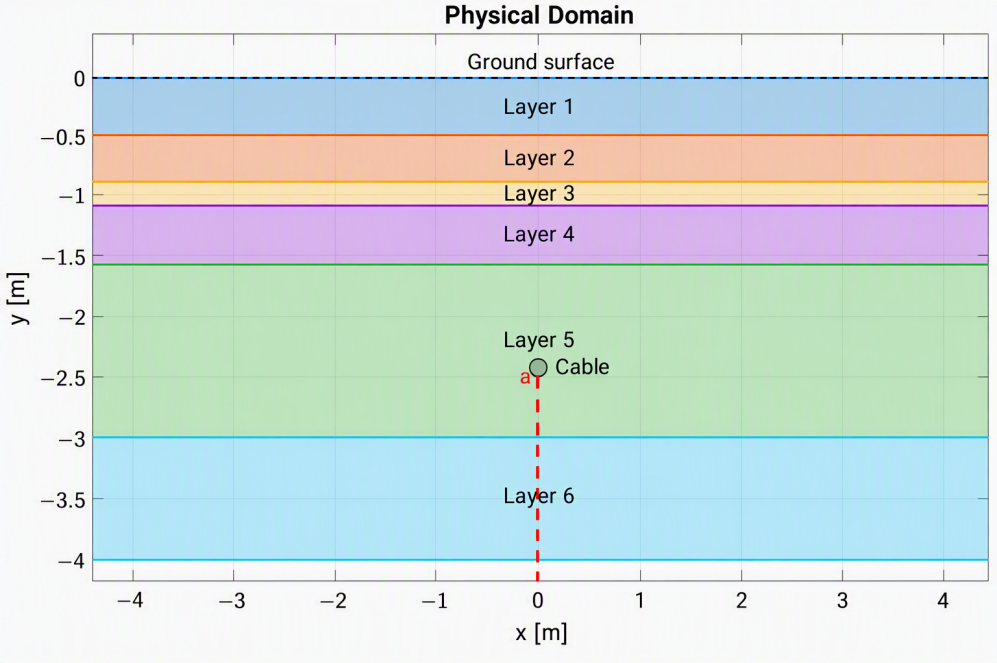


**Figure 4.** Physical domain of a single buried cable in a multilayer soil profile. The red dashed line indicates the branch cut of the logarithmic mapping and starts from point "a", located at the bottom centre of the cable surface.

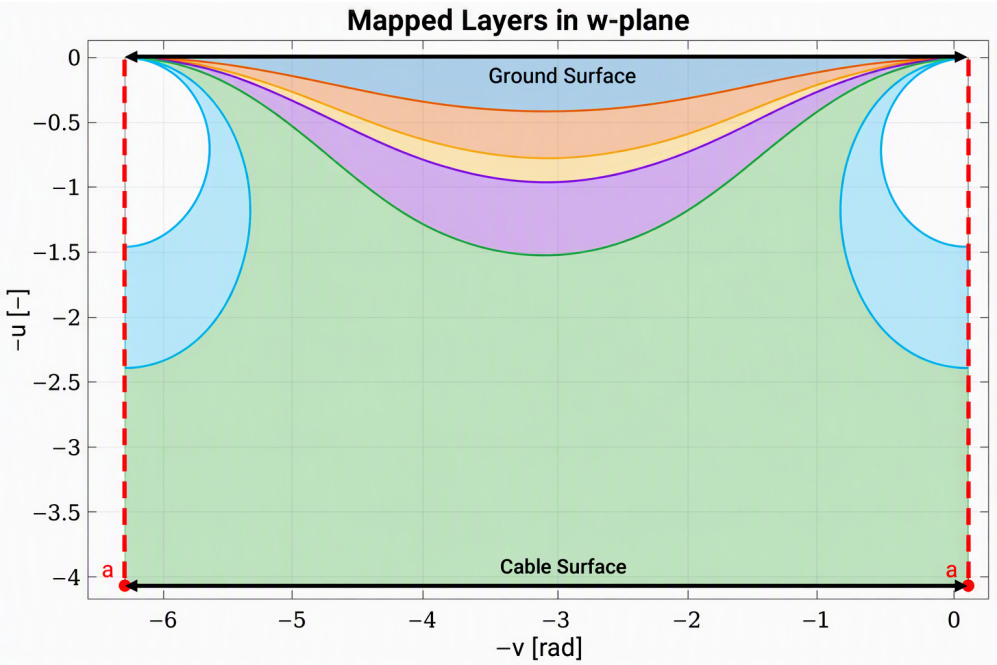


**Figure 5.** Transformed domain of the multilayer configuration obtained using conformal mapping. The colored lines represent the mapped boundaries between the different soil layers, and each mapped region is assigned the thermal resistivity of the corresponding soil layer. The two points labelled "a" correspond to the two mapped images of point "a" at the bottom centre of the cable surface.

*4.3. Numerical Implementation*

After the soil layers have been mapped into the transformed domain, the rectangular $u$-$v$ domain is discretised into a structured grid. Each grid cell is assigned the thermal resistivity of the mapped soil region in which it is located. The heat-transfer problem is then represented as an equivalent thermal resistance network. The steady-state heat conduction equation is:

$$\nabla \cdot \left( \frac{1}{\rho} \nabla \theta \right) = 0, \tag{7}$$

where $\theta$ is the temperature and $\rho$ is the local soil thermal resistivity. Since this equation is preserved under conformal mapping, the calculation can be performed in the transformed domain [8].

The thermal resistances between neighbouring nodes in the $u$- and $v$-directions are given by [8]:

$$r_u = \rho \left| \frac{u_e}{M-1} \frac{N}{2\pi} \right|, \tag{8}$$

and

$$r_v = \rho \left| \frac{2\pi}{N} \frac{M-1}{u_e} \right|, \tag{9}$$

where $M$ is the number of grid nodes in the $u$-direction and $N$ is the number of unique periodic nodes in the $v$-direction.

If a resistance element crosses a boundary between regions with different thermal resistivities, its effective resistivity is calculated according to the proportion of the element located in each region.

The cable and seabed surfaces are imposed as isothermal boundaries. The cable boundary is assigned the temperature $\theta_{\text{cable}}$, while the seabed boundary is assigned the ambient temperature $\theta_{\text{amb}}$.

In contrast, the two lateral boundaries of the transformed domain are not physical boundaries but represent the same physical line in the original domain. Therefore, the temperature field is periodic, with $\theta_{m,0} = \theta_{m,N}$. Since nodes $n = 0$ and $n = N$ coincide, only $N$ unique nodes are stored, indexed from $n = 0$ to $n = N - 1$. Periodicity is imposed by connecting node $n = N - 1$ directly to node $n = 0$, forming a closed resistance network in the $v$-direction.

For each node not located on the cable or seabed surfaces, the unknown temperature is determined by balancing the heat exchanged with the four neighbouring nodes. Defining the thermal conductances as $g_i = 1/r_i$, the resulting discrete equation is:

$$(g_1 + g_2 + g_3 + g_4)\theta_{m,n} - g_1\theta_{m-1,n} - g_2\theta_{m+1,n} - g_3\theta_{m,n-1} - g_4\theta_{m,n+1} = 0. \tag{10}$$

For the nodes directly below the seabed surface, at $m = 1$, the neighbouring temperature above is $\theta_{m-1,n} = \theta_{\text{amb}}$, while for the nodes directly above the cable surface, the neighbouring temperature below is $\theta_{m+1,n} = \theta_{\text{cable}}$. These prescribed temperatures are included in the heat-balance equations and moved to the right-hand side. Applying the heat balance to all unknown nodes gives the linear system:

$$\mathrm{A}\theta = \mathrm{b}, \tag{11}$$

where A is the conductance matrix, $\theta$ contains the unknown nodal temperatures, and b contains the contributions from the prescribed boundary temperatures.

In the original ELECTRA method, the nodal temperatures are obtained using an iterative Successive Over-Relaxation procedure [8]. In this work, the same resistance-network formulation is retained, but the equations are assembled into a sparse linear system and solved directly using Python 3.15.2.

## 5. Validation and Sensitivity Analysis

Before applying the proposed method to route-wide soil profiles, the numerical implementation was assessed through a grid-independence study and validated against finite-element simulations. Additional sensitivity analyses were then performed to evaluate the influence of far-field soil assumptions, lateral variability, solver parameters, and the isothermal cable-surface assumption.

### *5.1. Grid-Independence Study*

A grid-independence study was performed using the soil profile shown in Figure 4, where the soil layers, starting from the seabed surface, were assigned thermal resistivities of 0.4, 0.5, 0.6, 0.7, 0.8, and 0.9 K m/W, respectively. The numbers of nodes in the $u$- and $v$-directions were refined simultaneously using square grids from 50 × 50 to 400 × 400. This study was conducted for cable burial depths of 1.0 and 2.4 m, and convergence was evaluated from the relative change in equivalent thermal resistivity between consecutive grids.

As shown in Table 1, all relative changes are below the adopted convergence criterion of 0.1%. The slightly greater sensitivity of the 1.0 m case is attributed to the cable being located at the interface between two soil layers, making the representation of the material discontinuity more dependent on grid resolution.

**Table 1.** Grid-independence study for cable burial depths of 1.0 and 2.4 m using the soil profile shown in Figure 4.

| Grid $M \times N$ | Unknowns | $\rho_{\text{eff}}$, 1.0 m [K m/W] | Change [%] | $\rho_{\text{eff}}$, 2.4 m [K m/W] | Change [%] |
|---|---|---|---|---|---|
| 50 × 50 | 2400 | 0.5763 | – | 0.7236 | – |
| 100 × 100 | 9800 | 0.5766 | 0.0477 | 0.7237 | 0.0062 |
| 200 × 200 | 39,600 | 0.5766 | 0.0076 | 0.7236 | 0.0057 |
| 400 × 400 | 159,200 | 0.5766 | 0.0013 | 0.7236 | 0.0003 |

Refining the selected 200 × 200 grid to 400 × 400 changed the equivalent thermal resistivity by only 0.0013% for the 1.0 m burial depth and 0.0003% for the 2.4 m burial depth. These differences provide an estimate of the remaining discretisation error and indicate that the numerical solution is essentially grid independent.

The calculations presented in this study were therefore performed using $M = 200$ and $N = 200$, corresponding to $(M-2)N = 39{,}600$ unknown nodal temperatures. For this grid, the estimated 1-norm condition numbers of the sparse coefficient matrix were $3.96 \times 10^4$ and $5.00 \times 10^4$ for burial depths of 1.0 and 2.4 m, respectively. The corresponding normalised residuals were $3.56 \times 10^{-15}$ and $4.06 \times 10^{-15}$. These results indicate that the linear systems are well resolved and that numerical round-off or matrix-conditioning effects have a negligible influence on the calculated equivalent thermal resistivities.

### *5.2. Validation Against COMSOL*

Following the grid-independence study, finite-element simulations performed in COMSOL Multiphysics were used as a reference to validate the conformal-mapping-based solver.

The objective of this analysis was to verify whether the developed solver can reproduce the equivalent thermal resistivity obtained from a numerical model in which the layered soil profile is represented explicitly.

COMSOL was used as a reference model because it allows the soil stratigraphy and cable geometry, to be modelled directly. The validation was performed using representative soil-layer profiles derived from the available investigation data, so that the comparison was based on realistic seabed conditions.

COMSOL does not directly provide an equivalent thermal resistivity for a layered soil profile. Therefore, this value was obtained by comparing two simulations performed under the same loading and boundary conditions: a multilayer soil model and a homogeneous soil model. First, the multilayer model was simulated using the interpreted soil stratigraphy and the thermal resistivity assigned to each layer. A fixed current was applied to the cable, and the resulting conductor temperature was calculated. This temperature was then used as the reference thermal response of the layered seabed profile. A second model was created with the same cable geometry, burial depth, applied current, and boundary conditions, but with the surrounding soil represented as a homogeneous medium. The thermal resistivity of the homogeneous soil was adjusted iteratively until its conductor temperature matched that obtained from the multilayer model. The resulting homogeneous-soil value was taken as the COMSOL estimate of the equivalent thermal resistivity defined in Section 3. To reduce the number of finite-element simulations, the iterative procedure was stopped when the difference between the conductor temperatures obtained from the multilayer and homogeneous models was lower than 0.1 °C. This tolerance was considered sufficiently small for comparing the COMSOL results with those obtained using the developed conformal-mapping solver.

#### 5.2.1. COMSOL Reference Model

In the COMSOL reference model, heat transfer within the soil was assumed to occur by conduction only. The seabed surface was modelled as an isothermal boundary with a fixed temperature of 10 °C, while the outer boundaries of the soil domain were defined as adiabatic boundaries.

Although COMSOL provides infinite-element capabilities, a large finite soil domain was used in this study to simplify the automation of the parametric simulations in MATLAB R2026b. The domain was defined with a width and height of 200 m. This size was selected so that the outer boundaries were sufficiently far from the cable and their influence on the calculated conductor temperature remained negligible.

To verify this assumption, the results obtained with the 200 m finite domain were compared with an infinite-domain reference case. The difference in conductor temperature was found to be lower than 0.05 °C. This value is smaller than the 0.1 °C convergence tolerance used to determine the equivalent thermal resistivity in COMSOL. Therefore, the error introduced by using a large finite domain instead of an infinite domain is considered negligible for the purpose of this validation.

Two COMSOL reference configurations were considered, differing only in the representation of the cable. In the first configuration, the cable was modelled as a simplified circular isothermal boundary, consistent with the assumptions adopted in the conformal-mapping solver. This configuration allows for a direct comparison between the developed solver and a finite-element model based on the same idealised cable geometry.

In the second configuration, the soil profile, burial depth, boundary conditions, and loading conditions were kept unchanged, but the cable was represented using the full manufacturer geometry. Each layer was assigned its corresponding diameter and thermal resistivity, according to the manufacturer data. This allowed the thermal resistance inside the cable itself to be represented more realistically than in the simplified isothermal-cable model.

The material properties and outer diameters of the cable layers implemented in the COMSOL full-geometry model are summarised in Table 2. The corresponding cable cross-section is shown in Figure 6.

**Table 2.** Cable layer properties implemented in the COMSOL full-geometry model.

| Layer | Material Description | Outer Diameter (mm) | Thermal Conductivity ($W\,m^{-1}\,K^{-1}$) |
|---|---|---|---|
| Conductor | Stranded copper wires | 64.8 | 237 |
| Conductor screen | XLPE with carbon black | 68.8 | 0.27 |
| Insulation | XLPE | 122.8 | 0.27 |
| Insulation screen | XLPE with carbon black | 125.8 | 0.27 |
| Metallic screen | Aluminium sheath | 133.3 | 35 |
| Semiconducting sheath | XLPE with carbon black | 138.3 | 0.29 |
| Armour | Galvanised steel | 148.7 | 50 |
| Outer serving | PVC | 156.7 | 0.17 |

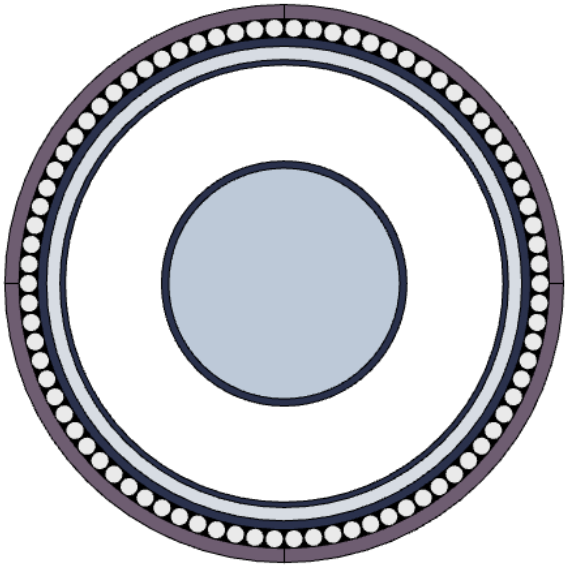

**Figure 6.** Cable cross-section implemented in the COMSOL full-geometry reference model.

This second configuration was included to assess how the additional geometric details of a realistic cable model influence the calculated equivalent thermal resistivity. By comparing the simplified isothermal-cable model with the full manufacturer-geometry model, the effect of the assumptions introduced in the conformal-mapping solver could be evaluated. This provides a direct check of whether the simplified cable representation introduces a significant error in the equivalent thermal resistivity calculation.

#### 5.2.2. Comparison Between COMSOL and the Conformal-Mapping Solver

After the equivalent thermal resistivity values were obtained from the COMSOL simulations, they were compared with the values calculated using the conformal-mapping solver. The same soil-layer profiles, burial depths, and thermal resistivity assignments were used in both methods to ensure a consistent comparison. The equivalent thermal resistivity values obtained for the 198 investigation locations using the three modelling approaches are compared in Figure 7.

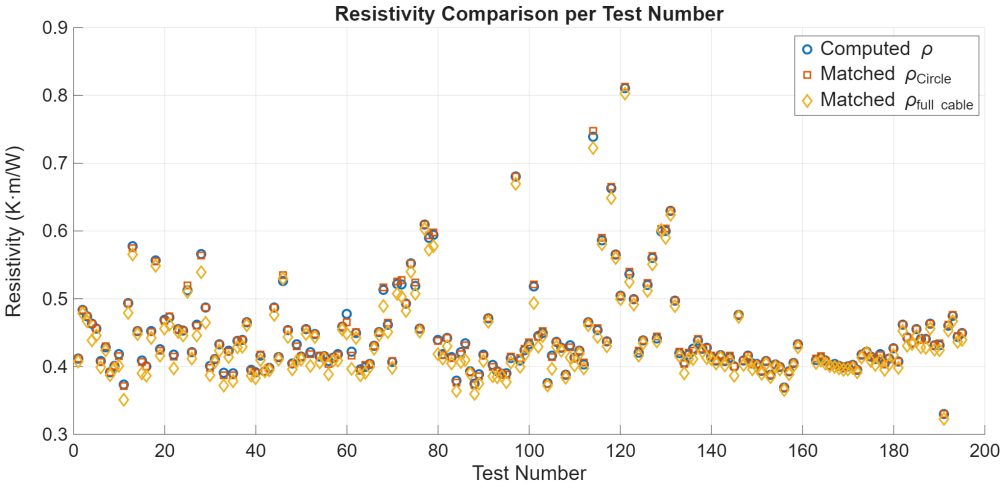


**Figure 7.** Equivalent thermal resistivity obtained at the 198 investigated locations using the proposed conformal-mapping solver and the COMSOL circular-isothermal-boundary and full-cable finite-element models. The analysed profiles cover burial depths of 1.7–6.8 m and assigned soil thermal resistivities of 0.27–2.2 K m/W. Each point represents one investigation location, with identical soil profiles and burial depths used in all three methods.

The comparison shows good agreement between the developed conformal-mapping solver and the COMSOL simulations. As shown in Figure 8, the difference between the developed solver and the COMSOL circular isothermal-boundary model remains below approximately 2%. This confirms that the conformal-mapping implementation is consistent with the finite-element solution when the same simplified cable representation is used.

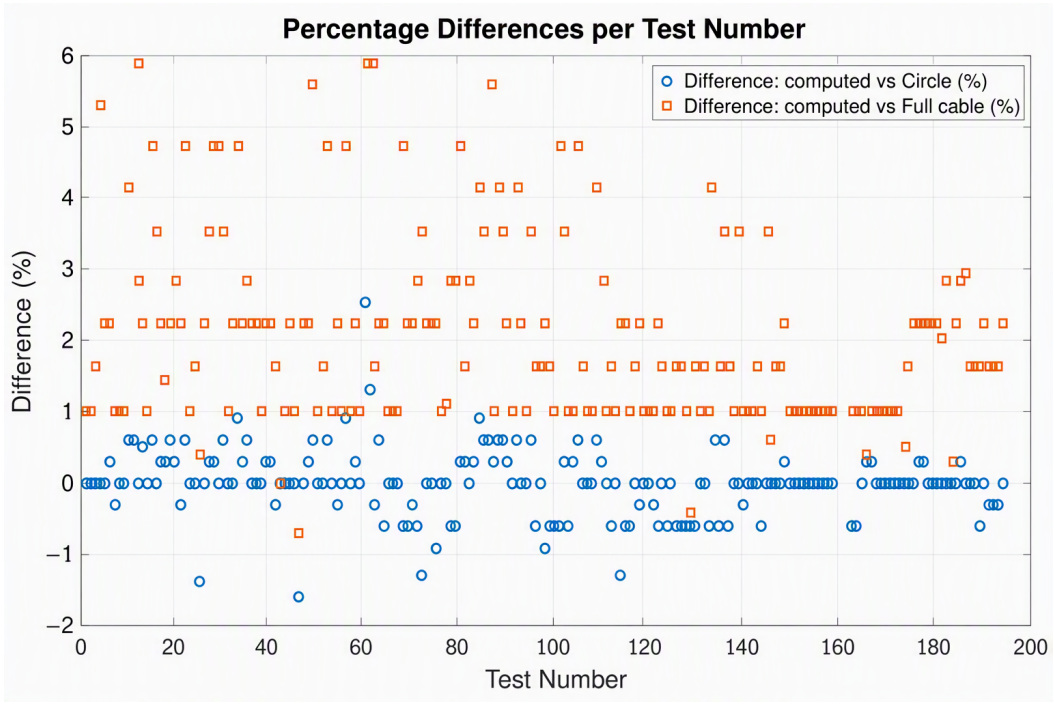


**Figure 8.** Percentage differences between equivalent thermal resistivity values obtained using the proposed conformal-mapping solver and the COMSOL circular-isothermal-boundary and full-cable finite-element models for 198 investigation locations. The analysed profiles cover burial depths of 1.7–6.8 m and assigned soil thermal resistivities of 0.27–2.2 K m/W. The COMSOL matching tolerance was 0.1 °C.

When the developed solver is compared with the COMSOL full-cable model, the maximum difference increases to approximately 6%. This larger deviation is expected,

because the full-cable model includes the detailed cable geometry and internal thermal layers, which are not represented in the simplified model considered in the conformal-mapping solver.

It can also be observed that some percentage differences appear in similar or repeated ranges. This behaviour is mainly caused by the numerical procedure used in COMSOL to determine the equivalent thermal resistivity, rather than by a physical effect. In the COMSOL procedure, the homogeneous soil resistivity was adjusted using a bisection method, starting from the equivalent thermal resistivity obtained with the developed conformal-mapping solver. The iteration was stopped when the conductor temperature of the homogeneous model matched the multilayer case within a prescribed tolerance. As a result, the final accepted values are selected from discrete numerical steps around the initial estimate, which explains the repeated percentage-difference levels.

Overall, the validation confirms that the proposed conformal-mapping-based method provides reliable estimates of equivalent thermal resistivity for layered soil profiles. The method reproduces the COMSOL reference results with good accuracy, while avoiding the need for repeated finite-element simulations for each investigation location and burial depth.

### *5.3. Influence of Cable Diameter and Isothermal Cable-Surface Assumption*

Following the validation against COMSOL, additional checks were performed to assess the influence of the equivalent circular cable diameter and the isothermal cable-surface assumption adopted in the conformal-mapping solver. These parameters may introduce uncertainty during the early stages of an offshore cable project, when the final cable design may not yet be available. The equivalent circular cable diameter determines the size of the isothermal cable boundary and therefore influences the total heat flow between the cable and the surrounding soil. However, its influence on the calculated equivalent thermal resistivity remains limited. As shown in Figure 9, variations in cable diameter produce only small changes in $\rho_{eq}$, typically in the second decimal place. Even a fourfold increase in diameter results in a change of approximately 3%.

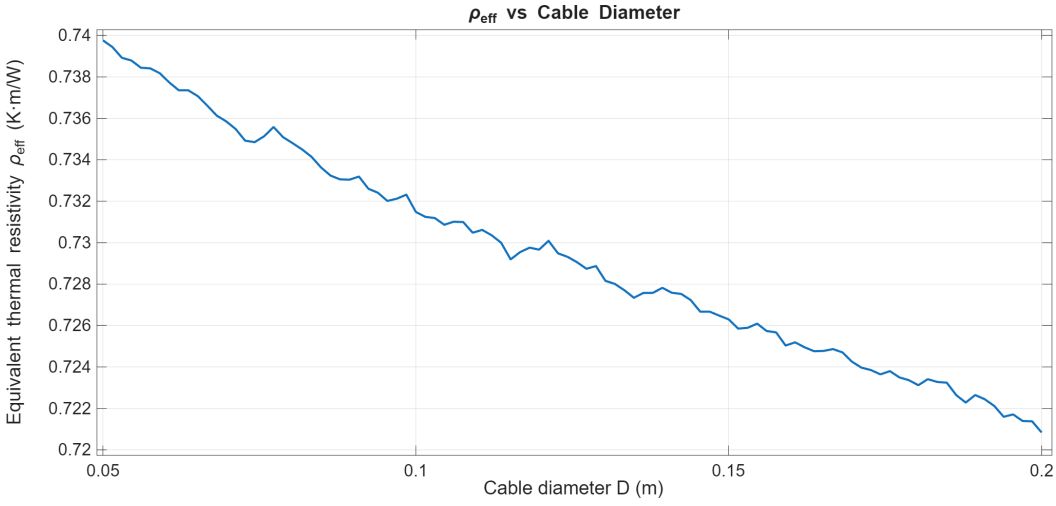


**Figure 9.** Equivalent thermal resistivity calculated with the proposed conformal-mapping solver as a function of the external cable diameter. The layered soil profile shown in Figure 4 was used, with thermal resistivities of 0.4, 0.5, 0.6, 0.7, 0.8, and 0.9 K m/W assigned consecutively from the seabed surface downwards. The cable burial depth was fixed at 2.4 m, while the soil-layer geometry and assigned thermal resistivities were kept constant throughout the analysis.

This result indicates that the conformal-mapping solver is only weakly sensitive to uncertainties in the equivalent cable diameter. The method can therefore be applied during

early-stage assessments when the final cable dimensions are not yet defined. The isothermal cable-surface assumption was verified by comparison with COMSOL simulations. In the conformal-mapping solver, the cable is represented as a circular boundary with a uniform temperature. To assess this simplification, the temperature distribution along the actual cable surface was extracted from COMSOL using the full cable configuration described in Section 5.2. Two configurations were analysed. In the first case, the cable was embedded within a single soil layer and located sufficiently far from the surrounding layer interfaces. The temperature variation along the cable surface was below 0.15 °C, indicating that the cable surface was nearly isothermal. The equivalent thermal resistivity obtained with the developed solver was 0.580 K m/W, while COMSOL gave 0.585 K m/W, confirming very good agreement. In the second case, the cable was placed directly at the interface between two soil layers with a strong thermal contrast. This represents a more critical configuration because different parts of the cable surface are surrounded by materials with different thermal resistivities. The temperature variation along the cable surface increased to approximately 2 °C. Nevertheless, the equivalent thermal resistivity obtained with the developed solver was 0.75 K m/W, compared with 0.77 K m/W from COMSOL. The corresponding difference in conductor temperature was approximately 0.6 °C. These results show that the isothermal cable-surface assumption is well satisfied when the cable is embedded within a single soil layer. Even when the cable is located at an interface between two contrasting layers, the difference between the developed solver and COMSOL remains small. The isothermal cable-surface assumption therefore introduces only a minor error for the analysed configurations. Overall, the equivalent cable diameter and isothermal cable-surface assumption have only a limited influence on the calculated equivalent thermal resistivity. The following analyses therefore focus on uncertainties associated with the soil domain, including the extent of the thermally relevant region and the treatment of unmeasured soil farther from the cable.

### *5.4. Influence of Far-Field Soil*

After validating the numerical approach and assessing the main conformal-mapping assumptions, the influence of the far-field soil was investigated. The objective was to determine the extent of the soil region around the cable that significantly contributes to heat dissipation and, consequently, to the conductor temperature.

This is relevant for offshore cable applications because soil information is only available within a limited region around each investigation location. Thermal resistivity measurements and stratigraphic descriptions typically extend to about 5–6 m below the seabed, while the lateral size of a vibrocore sample is only of the order of 10 cm. As a result, the soil is well characterised only within a narrow vertical column, whereas the surrounding soil remains uncertain.

To assess this effect, the soil domain was divided into a relevant-soil region surrounding the cable and a far-field soil region outside it. These regions were assigned thermal resistivities of $\rho_{\mathrm{rel}} = 0.4$ K m/W and $\rho_{\mathrm{far}} = 2.0$ K m/W, respectively. This strong contrast was selected to identify the extent of soil that significantly influences the conductor temperature. Separate vertical and horizontal sensitivity analyses were performed by progressively increasing the relevant-soil region in the corresponding direction.

A 98% criterion was used to define the approximate extent of the thermally relevant soil region. This threshold was reached when 98% of the total temperature reduction had occurred compared with the final plateau value. Beyond this point, further enlargement of the relevant soil region was considered to have only a minor influence on the conductor temperature.

In the vertical sensitivity study, the relevant-soil region was rectangular and extended over the full width of the numerical domain. Its initial vertical extent reached from the seabed surface to the lower surface of the cable. The region was then progressively extended below the cable, while all soil beneath it was defined as far-field soil. The parameter $\Delta H_{\mathrm{rel}}$ represents the increase in the height of the relevant-soil region below the cable. The resulting variation in conductor temperature is shown in Figure 10.

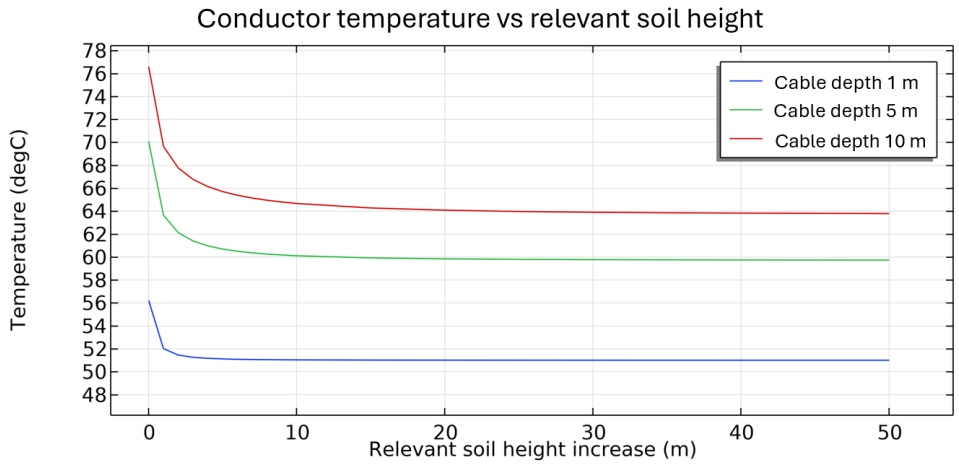


**Figure 10.** Effect of increasing the height of a low-resistivity relevant-soil region on conductor temperature obtained from COMSOL simulations.

The results in Figure 10 and Table 3 show that the conductor temperature decreases as the low-resistivity region is extended below the cable. However, the reduction becomes progressively smaller with increasing distance from the cable. Once the 98% threshold is reached, the remaining far-field soil has only a minor influence on the conductor temperature.

**Table 3.** Increase in relevant-soil height required to reach the 98% temperature-reduction criterion in the vertical sensitivity study.

| Curve | $\Delta H_{\mathrm{rel}}$ [m] | Percentage of Total Drop |
|---|---|---|
| Curve 1 | 14 | 98.42% |
| Curve 2 | 15 | 98.03% |
| Curve 3 | 30 | 99.08% |

In the horizontal sensitivity study, the relevant-soil region was rectangular and extended over the full height of the numerical domain. Its lateral boundaries were progressively moved outward by equal distances from the cable centreline, while the soil outside these boundaries was defined as far-field soil. The parameter $\Delta W_{\mathrm{rel}}$ represents the increase in the total width of the relevant-soil region. The resulting variation in conductor temperature is shown in Figure 11.

The horizontal sensitivity results in Figure 11 and Table 4 show the same general trend. The conductor temperature decreases rapidly when the soil immediately surrounding the cable is included in the low-resistivity region. As the relevant region is extended farther away from the cable, the additional reduction in temperature becomes smaller. Compared with the vertical case, a larger extent is required in the horizontal direction before the temperature approaches a plateau, indicating that heat spreads laterally over a wider soil volume.

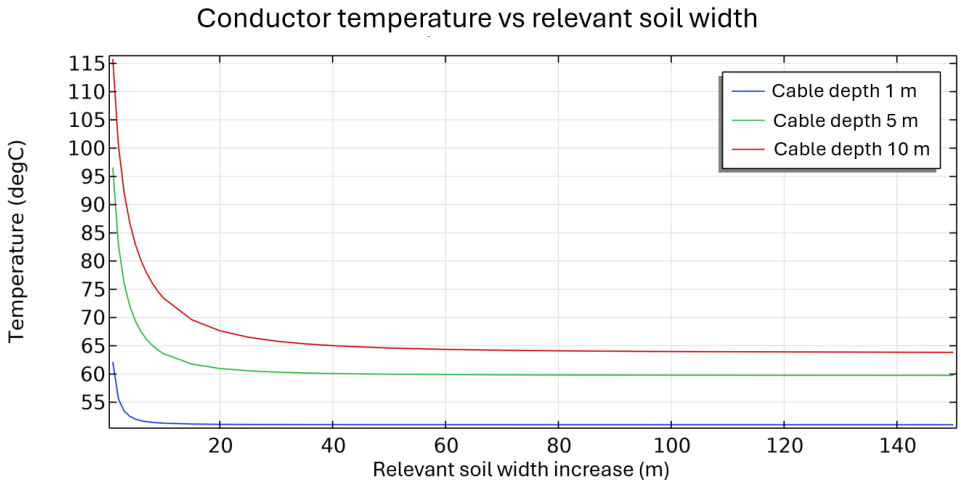


**Figure 11.** Effect of increasing the width of a low-resistivity relevant-soil region on conductor temperature obtained from COMSOL finite-element simulations.

**Table 4.** Increase in relevant-soil width required to reach the 98% temperature-reduction criterion in the horizontal sensitivity study.

| Curve | $\Delta W_{\mathrm{rel}}$ [m] | Percentage of Total Drop |
|---|---|---|
| Curve 1 | 15 | 98.92% |
| Curve 2 | 30 | 98.45% |
| Curve 3 | 50 | 98.52% |

Overall, the height and width sensitivity studies confirm that the soil closest to the cable has the strongest influence on the thermal response. The influence of the surrounding soil decreases gradually with distance, and beyond the 98% threshold, further enlargement of the characterised soil region has only a minor effect on the conductor temperature. This indicates that the thermally relevant region is larger than the soil volume directly sampled by vibrocores, but that far-field soil assumptions become less important once the cable remains within or close to a sufficiently characterised soil interval.

### *5.5. Sensitivity to Far-Soil Assumptions for Real Soil Profiles*

The previous idealised COMSOL sensitivity study showed that the soil region influencing the conductor temperature can be larger than the soil volume directly characterised by geotechnical investigations. This means that, in principle, part of the soil contributing to heat dissipation may lie outside the region where thermal resistivity measurements are available. However, the previous analysis was intentionally performed using a strong thermal contrast between the relevant soil and the far-field soil, with the far-field thermal resistivity set to 2.0 K m/W. This value is very high for typical saturated offshore seabed conditions and was mainly used to clearly identify the distance beyond which the far-field soil has almost no influence on conductor temperature.

For this reason, a second sensitivity analysis was performed using the real interpreted soil profiles along the cable route. The aim was to evaluate whether realistic assumptions for the far-field soil thermal resistivity significantly affect the equivalent thermal resistivity calculated with the developed conformal-mapping tool. In this analysis, the cable was represented as an isothermal circular boundary, consistent with the assumptions of the conformal-mapping solver.

For each investigation location, the interpreted layered soil profile was assumed to extend 20 m horizontally, corresponding to 10 m on each side of the cable. This project-specific assumption is considered reasonable for the Dutch sector of the North Sea, where

the soil stratigraphy was formed by large-scale fluvial, deltaic, glacial, tidal, and marine depositional processes that generally produce layers extending laterally beyond the width of an individual sample [20,21]. However, local lateral variations may still occur; therefore, the influence of this assumption is investigated separately in Section 5.6.

In the vertical direction, the interpreted profile was extended 0.30 m below the deepest available thermal resistivity measurement, which was performed at the end of the recovered sample. This project-specific extension was selected because the identified soil layers generally extended over several tens of centimetres or more, making it unlikely that the deepest layer terminated exactly at the end of the sample. The extension was kept limited to avoid assigning the measured thermal resistivity to a large uninvestigated region.

Outside this defined layered region, both laterally and below the interpreted profile, the soil was treated as homogeneous far-field soil with a fixed thermal resistivity. To assess the influence of this assumption, two simulations were performed for each investigation location and burial depth. In the first case, the far-field soil thermal resistivity was set to:

$$\rho_{\text{far}} = 0.4\,\text{K m/W}, \tag{12}$$

while in the second case, it was set to:

$$\rho_{\text{far}} = 1.0\,\text{K m/W}. \tag{13}$$

These values were selected based on the measured thermal resistivity distribution along the investigated route. Most samples consisted of sand, with values generally between 0.4 and 0.5 K m/W, while values of 1.0 K m/W or higher, representative of clayey soils, occurred in less than 5% of the measurements. Therefore, 0.4 and 1.0 K m/W were selected as realistic favourable and unfavourable bounds, respectively. The equivalent thermal resistivity was then calculated for both cases, and the percentage difference between the two results was used to quantify the sensitivity of the model to the far-soil assumption.

The results in Figure 12 show that, for the burial depths relevant to the project, the influence of the far-field soil assumption is limited. At a burial depth of approximately 5 m, the maximum difference between the two assumed far-field thermal resistivity values is about 5%. This indicates that, under the considered installation conditions, the equivalent thermal resistivity is governed mainly by the interpreted soil profile surrounding the cable, while the soil outside this region has a smaller influence.

The influence of the assumed far-field soil properties increases at greater burial depths. As the cable is installed deeper, it approaches the lower boundary of the measured and interpreted soil profile. Consequently, the far-field soil region is no longer located far from the cable but lies in its immediate proximity and contributes more directly to heat dissipation. The thermal resistivity assigned to this region therefore has a greater influence on the calculated equivalent thermal resistivity.

This effect is evident at the two cable-route locations where the burial depth exceeds approximately 5 m. At these locations, the cable is situated below the lower boundary of the interpreted soil profile and is therefore embedded in the far-field soil region. Changing the thermal resistivity assigned to the far-field soil consequently changes the thermal properties of the material directly surrounding the cable. The resulting larger variation in equivalent thermal resistivity is therefore expected and is consistent with the model configuration. Based on the investigated profiles, the method is considered applicable without additional far-field treatment when the cable remains within the measured and interpreted soil profile, which generally corresponds to burial depths up to approximately 5 m for the present dataset. For deeper burial depths, the influence of the uncharacterised far-field soil may increase, as indicated by the vertical and horizontal sensitivity analyses in Figures 10 and 11. The 5 m value is therefore project-specific and should not be interpreted as a general limit of

the method. When the cable extends below the investigated profile, additional site-specific measurements should be obtained where possible. Otherwise, conservative assumptions should be adopted for the uncharacterised soil, including the use of an upper representative thermal resistivity value for the far-field region.

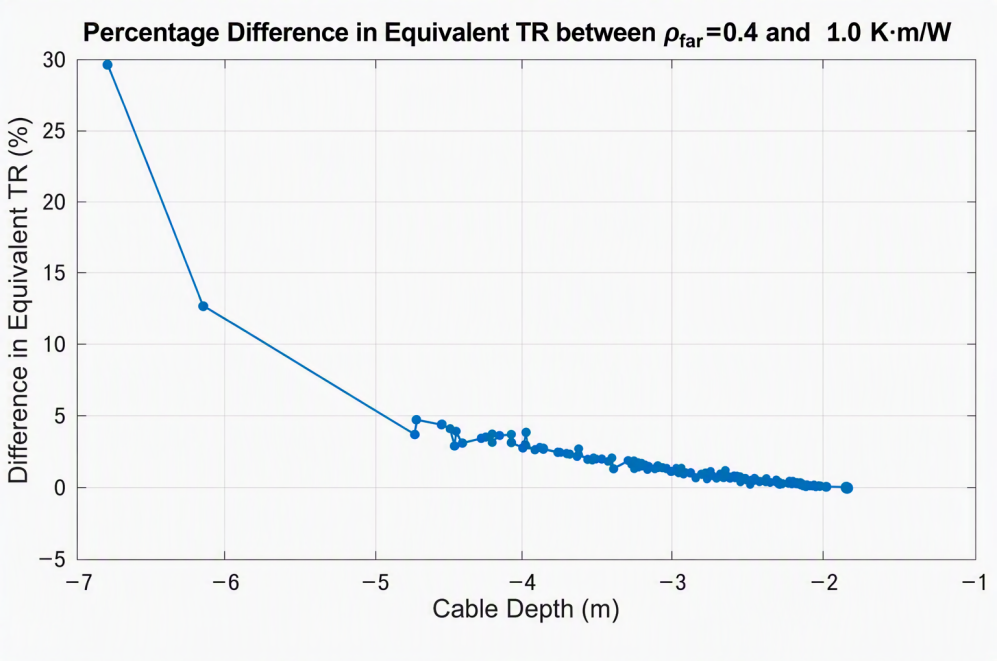


**Figure 12.** Influence of the assumed far-soil thermal resistivity on the equivalent thermal resistivity calculated with the proposed conformal-mapping solver for 198 real soil profiles. The assigned soil thermal resistivities range from 0.27 to 2.2 K m/W.

### *5.6. Influence of Lateral Soil Variability*

The preceding analysis assumed that the interpreted soil conditions were laterally constant within the defined layered region. However, local variations, including isolated zones of peat, clay, gas-bearing sediment, organic material, or other high-resistivity soil, may not be captured by the available geotechnical and thermal investigations. If located close to the cable, such variations could locally reduce heat dissipation and increase the conductor temperature.

To assess the sensitivity to this assumption, local high-resistivity inclusions were introduced within the layered region. The analysis examined whether an unfavourable soil inclusion near the cable could significantly affect the conductor temperature and the calculated equivalent thermal resistivity. A high-resistivity inclusion was introduced beside the cable in a relatively homogeneous low-resistivity soil profile selected from the measured profiles. Its vertical position, horizontal distance from the cable, thermal resistivity, and size were varied in separate parametric studies. This allowed the effects of both small local inclusions and larger unfavourable soil zones to be evaluated.

Initially, the inclusion was modelled as a square block with dimensions 1.2 m × 1.2 m and a thermal resistivity of 1.2 K · m/W. This value was selected to represent a local unfavourable material with poorer thermal performance than the surrounding soil. In the first part of the lateral variability analysis, the size and thermal resistivity of the inclusion were kept constant, while its vertical starting position and horizontal distance from the cable were varied. This first study was therefore intended to identify the most critical inclusion position and assess its influence on the conductor temperature.

Figure 13 shows the physical configurations considered in this initial part of the analysis. The coloured squares represent the different vertical starting positions of the high-resistivity

inclusion with respect to the cable centreline. The vertical offset is defined as the distance between the centre of the inclusion and the cable centre position. A negative offset indicates that the centre of the inclusion is located below the cable centreline, while a positive offset indicates that it is located above the cable centreline.

The same colour convention and vertical offset values are used in Figure 14, where each curve refers to one of the vertical positions shown in Figure 13. The conductor temperature and the corresponding equivalent thermal resistivity are shown on the left and right y-axes, respectively. For each vertical position, the inclusion was progressively shifted horizontally away from the cable. The horizontal axis therefore represents the lateral distance between the cable and the high-resistivity inclusion, allowing the combined influence of vertical position and horizontal distance to be evaluated.

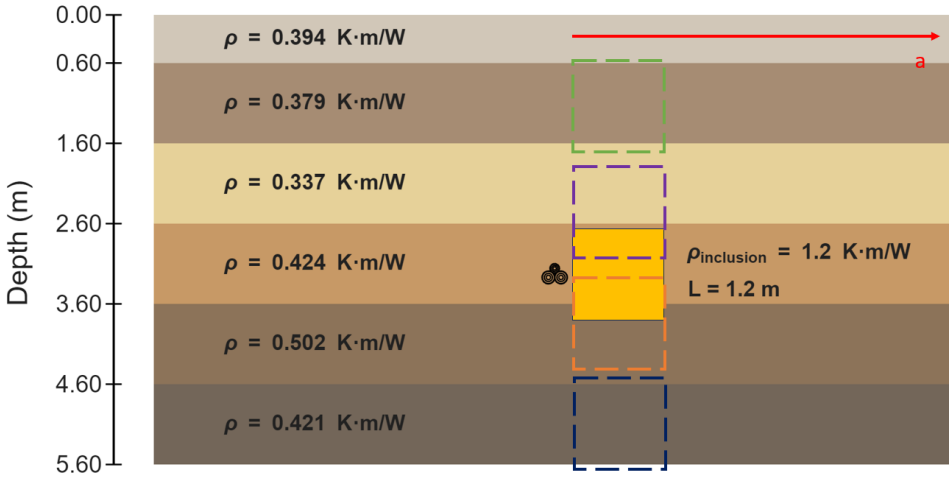


**Figure 13.** Configuration of the high-thermal-resistivity inclusion for the vertical-position parametric study. Point "a" identifies the cable-centre reference position, and the arrow indicates the horizontal direction in which the inclusion was shifted away from the cable. The different colours represent the investigated vertical offsets of the inclusion starting position relative to the cable centreline.

The results show that the high-resistivity inclusion has a limited effect on the conductor temperature. The highest temperature increase occurs when the inclusion is located directly next to the cable, especially when it is vertically aligned with the cable position. However, even in this most unfavourable configuration, the temperature increase is only slightly above 3 °C.

For all investigated vertical positions, the influence of the inclusion decreases rapidly as it is moved horizontally away from the cable. This shows that the thermal effect of a small high-resistivity zone is mainly governed by its proximity to the cable. When the inclusion is shifted upward or downward, the impact is further reduced because it moves away from the main heat-flow path.

Overall, the 1.2 m × 1.2 m inclusion considered in this initial study does not significantly affect the cable thermal response unless it is located very close to the cable.

A second parametric study was performed to evaluate the influence of the thermal resistivity of the inclusion. Based on the preceding analysis, the inclusion was placed in the most unfavourable investigated position, directly adjacent to the cable and vertically aligned with its centre. This position corresponds to the filled yellow square shown in Figure 13. The inclusion dimensions were kept constant at 1.2 m × 1.2 m, while its thermal resistivity was progressively increased from 0.4 to 2.0 K m/W. The results are presented in Figure 15.

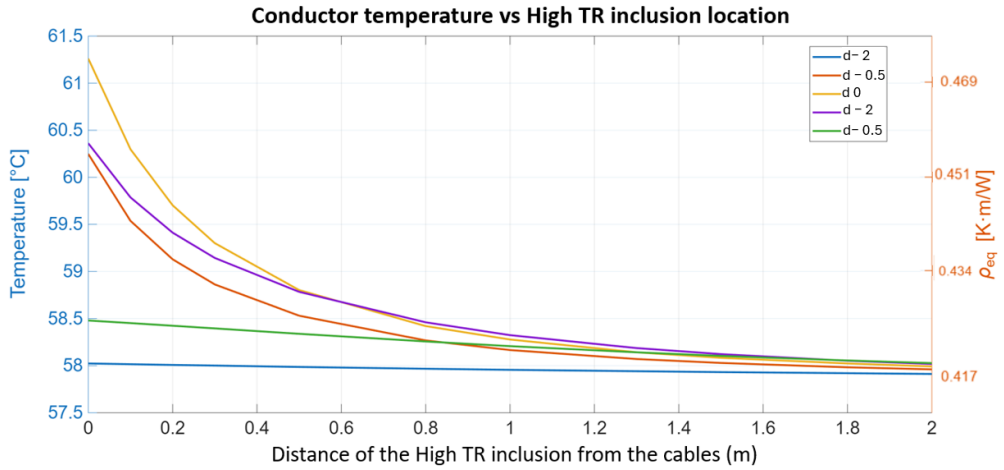


**Figure 14.** Conductor temperature and equivalent thermal resistivity obtained from COMSOL finite-element simulations as functions of the horizontal distance between the cable and a 1.2 m × 1.2 m high-resistivity inclusion, for the investigated vertical offsets. The inclusion thermal resistivity was fixed at 1.2 K m/W, and the cable burial depth was 2.4 m.

The results in Figure 15 show that increasing the thermal resistivity of the inclusion has only a limited effect on the conductor temperature. Even when the thermal resistivity is increased to 2.0 K · m/W, the temperature increase compared with the reference case of 1.2 K · m/W, for the same inclusion position, is only slightly above 1 °C. This indicates that, for the relatively small inclusion considered, increasing its resistivity has only a minor influence on the cable thermal response, since its limited size does not significantly disturb the overall heat dissipation around the cable.

For this reason, a third parametric study was carried out to evaluate the influence of the inclusion size. Starting from the position that produced the highest temperature increase, the dimensions of the high-resistivity region were progressively increased up to a 5 m × 5 m square while keeping the thermal resistivity fixed at 1.2 K · m/W. This value was maintained because higher thermal resistivity values are considered unlikely to occur in practice. The corresponding configuration and results are shown in Figures 16 and 17.

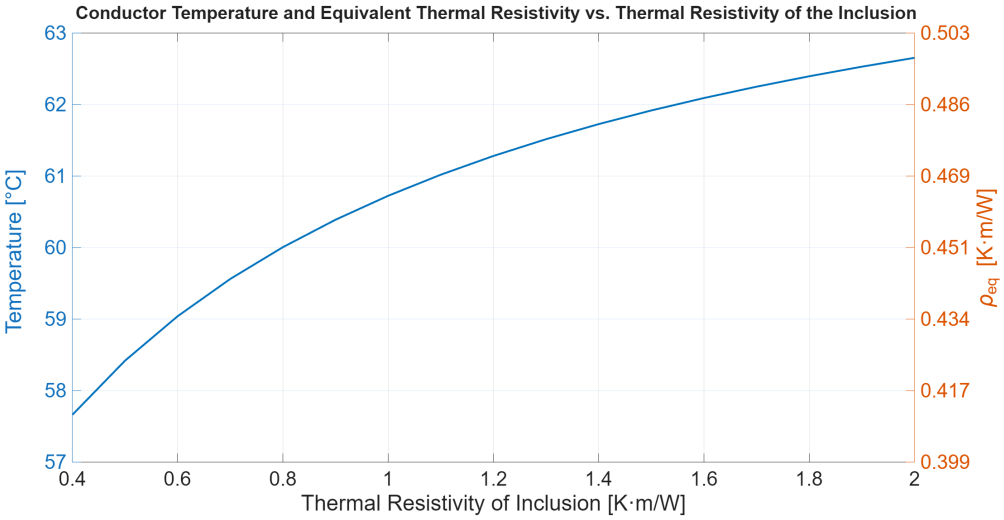


**Figure 15.** Conductor temperature and equivalent thermal resistivity obtained from COMSOL finite-element simulations as functions of the thermal resistivity of a 1.2 m × 1.2 m inclusion. The inclusion was positioned directly adjacent to and vertically aligned with the cable, as indicated by the filled yellow square in Figure 13. The cable burial depth was 2.4 m.

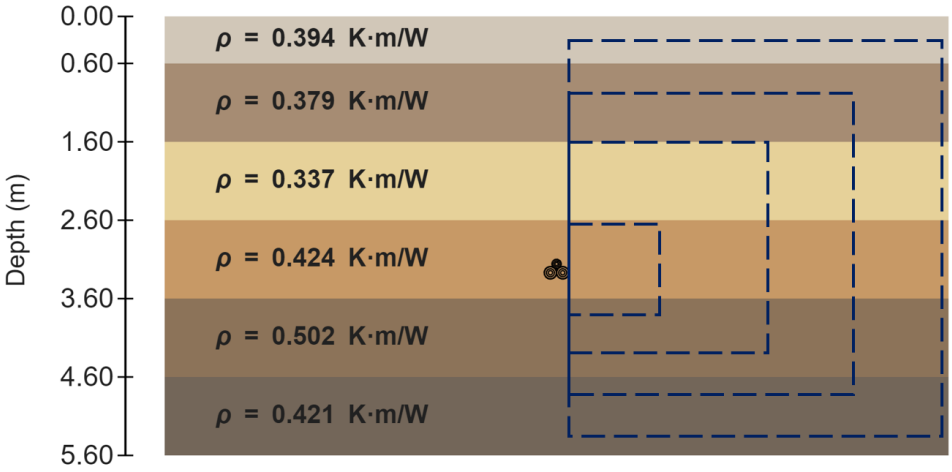


**Figure 16.** Square high-resistivity inclusions considered in the inclusion-size analysis. The dashed square boundaries represent the progressively increasing dimensions of the investigated inclusions. The inclusions were positioned directly adjacent to and vertically aligned with the cable, with a thermal resistivity of 1.2 K m/W. The cable burial depth was 2.4 m.

As expected, increasing the size of the inclusion leads to a higher conductor temperature, since a larger part of the heat-flow path is affected by the higher thermal resistivity. The largest temperature increase is obtained when the inclusion reaches its maximum considered size of 5 m × 5 m and is placed directly next to the cable.

This configuration is very conservative and unlikely to occur in practice. It assumes an abrupt lateral change from the measured low-resistivity soil to a large high-resistivity region immediately beside the cable. In addition, the thermal resistivity assigned to the inclusion is approximately three times higher than that of the surrounding measured soil. Even under these unfavourable assumptions, the conductor temperature increases by approximately 6 °C compared with the base scenario.

Since this larger inclusion gives a more noticeable temperature increase, an additional parametric study was performed to evaluate the effect of its horizontal position. The aim was to verify whether a large high-resistivity region would still influence the conductor temperature if it were not located directly beside the cable. For this purpose, the 5 m × 5 m high-resistivity block, corresponding to the largest dashed square shown in Figure 16, was progressively shifted away from the cable. The corresponding results are shown in Figure 18.

The influence of the 5 m × 5 m high-resistivity region decreases rapidly as it is moved away from the cable. At a distance of approximately 0.60 m, its effect on the conductor temperature is reduced by about half, while at distances greater than approximately 1.5 m, the effect becomes almost negligible. Within the investigated ranges of inclusion size, position, and thermal resistivity, small inclusions had a limited effect, while larger unfavourable zones became relevant mainly when located directly beside the cable or within the main heat-flow region. These findings apply only to the tested soil profile, cable configuration, burial depth, and inclusion properties and should not be generalised to other installation conditions.

For the specific configuration analysed, a potentially more significant source of uncertainty is the variation in soil layering and cable burial depth along the route. Although the cable may be located in thermally favourable soil at an investigation location, lateral changes in layer depth or thickness, combined with variations in burial depth, could result in the cable intersecting a material with substantially higher thermal resistivity between investigation locations. This situation may produce a greater increase in conductor temperature than an isolated inclusion and could lead to unexpected local thermal hotspots.

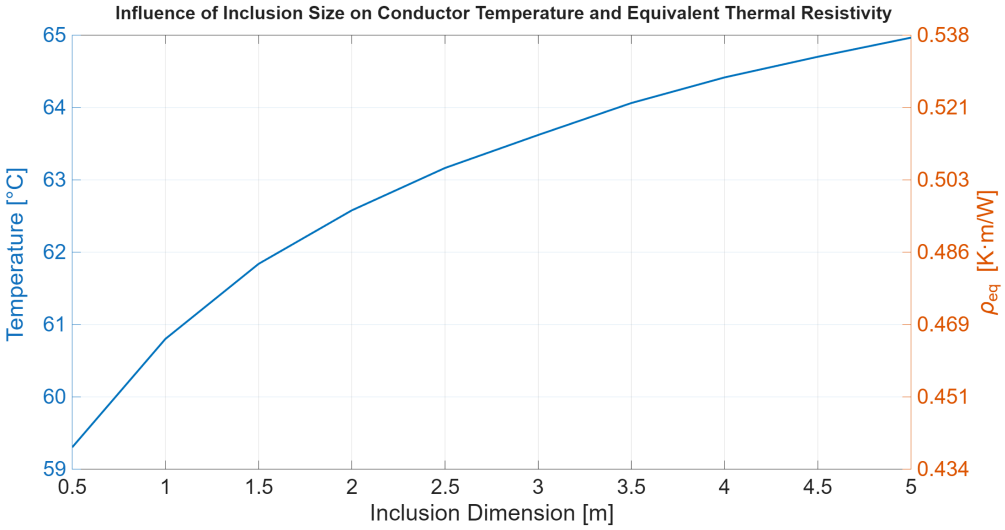


**Figure 17.** Conductor temperature and equivalent thermal resistivity obtained from COMSOL finite-element simulations as functions of the size of the square high-resistivity inclusion for the configurations shown in Figure 16. The inclusion was positioned directly adjacent to and vertically aligned with the cable, with a thermal resistivity of 1.2 K m/W. The cable burial depth was 2.4 m.

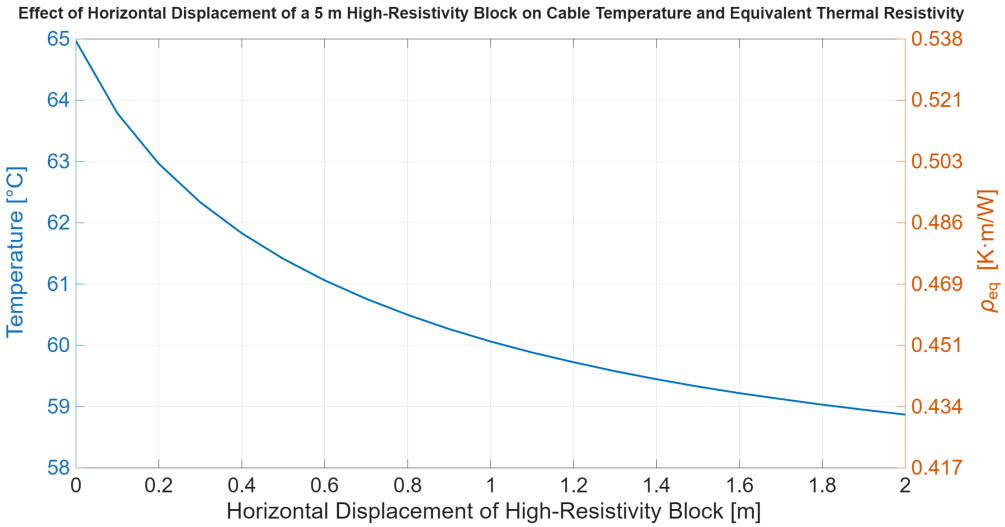


**Figure 18.** Conductor temperature and equivalent thermal resistivity obtained from COMSOL finite-element simulations as functions of the horizontal distance between the cable and the 5 m × 5 m high-resistivity inclusion. The inclusion thermal resistivity was fixed at 1.2 K m/W, and the cable burial depth was 2.4 m.

## 6. Real Case Scenario Analysis

After validating the developed method and investigating the main sources of uncertainty related to the soil domain, the approach was applied to selected soil configurations obtained from the site investigation data. The objective of this section is to illustrate how local soil stratigraphy, layer continuity, burial depth, and uncertainty in thermal resistivity can influence the calculated equivalent thermal resistivity and conductor temperature. Two representative cases are analysed. The first compares Locations A and B to evaluate the implications of variations in layer depth, thickness, continuity, and cable burial depth between nearby investigation locations. The second considers Location C, where an unmeasured thin peat layer is located close to the cable depth, to assess the possible thermal influence of a thin high-resistivity layer.

### *6.1. Locations A and B: Influence of Layer Continuity and Burial Depth*

Although the cable is located in relatively low-resistivity material at both Locations A and B, nearby high-resistivity layers introduce uncertainty in the interpretation of the soil conditions between the two investigation locations. Both locations lie on the expected cable route and are separated by a plan-view distance of approximately 572.14 m, with east–west and north–south coordinate differences of 396.10 m and 412.97 m, respectively.

Figure 19 compares the soil profiles at Locations A and B. For each location, the recovered sample is shown next to the interpreted stratigraphy. Yellow represents sand, blue represents clay, and green represents silty sand. The assigned thermal resistivity values are reported alongside the interpreted layers, while the cable position is indicated by the blue circle. The depth scale is referenced to Lowest Astronomical Tide (LAT), and a brief soil description is included for each location. The developed method gives equivalent thermal resistivity values of approximately 0.45 K m/W for Location A and 0.51 K m/W for Location B.

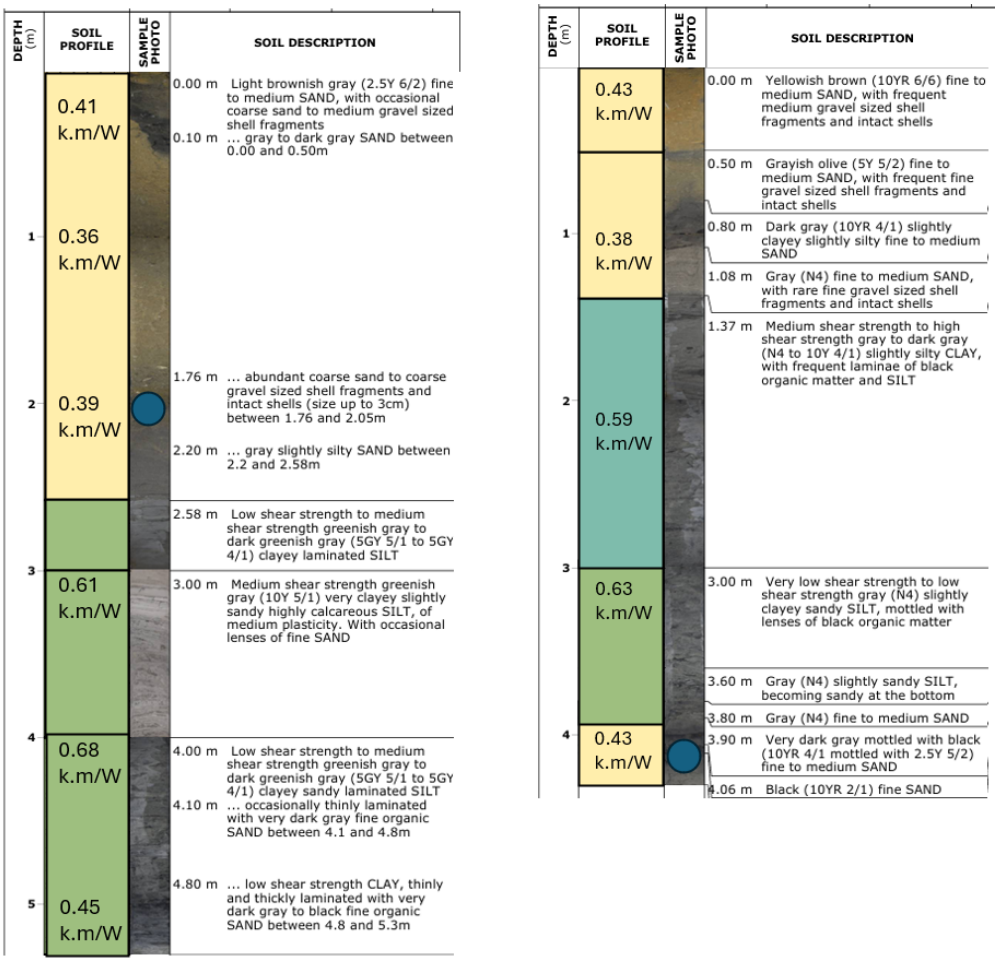


**Figure 19.** Soil stratigraphy at Locations A (**left**) and B (**right**). For each location, the recovered soil sample is shown together with the interpreted stratigraphic profile, assigned thermal resistivity values, and cable position.

In both profiles, a clay layer with higher thermal resistivity is located close to the cable. However, the equivalent thermal resistivity remains relatively low because the cable is not directly embedded in this material. At Location A, the cable is located approximately 0.30 m above the clay layer, while at Location B it is approximately 0.20 m below it. The cable is therefore mainly surrounded by lower-resistivity soil, which limits the influence of the nearby clay layer on the overall thermal response. The soil conditions between the two

locations remain uncertain. The high-resistivity layer may vary in depth or thickness along the route, while the cable burial depth increases from approximately 2 m to 4.1 m. Because this layer occurs within the same depth interval, the cable could locally intersect it between the two investigation locations, even though it is not directly embedded in it at either location. This could locally increase the equivalent thermal resistivity and potentially produce an unexpected thermal hotspot. This case highlights the importance of considering soil-layer continuity together with burial-depth variations along the route. Investigation locations should therefore not be interpreted independently, particularly when high-resistivity layers are located close to the planned cable depth.

### *6.2. Location C: Influence of a Thin High-Resistivity Layer*

Since no direct thermal resistivity measurement was available within the peat layer at Location C, its influence was assessed by varying its assumed thickness and thermal resistivity.

Figure 20 shows the recovered soil sample and the interpreted stratigraphy at Location C. As in the previous case, the colours indicate the main soil types and the blue circle represents the cable position. The thermal resistivity values assigned to the interpreted layers are also shown. Most of the profile consists of sandy material with relatively low thermal resistivity, while a thin peat layer is present close to the cable depth. To quantify the uncertainty associated with this unmeasured peat layer, a sensitivity analysis was performed by varying both its thickness and assigned thermal resistivity. The soil stratigraphy implemented in the numerical simulations is shown in Figure 21.

In Figure 22, the conductor temperature and equivalent thermal resistivity are shown on the left and right y-axes, respectively. The results show that the influence of the peat layer strongly depends on its position relative to the cable. When the cable is located within or very close to a high-resistivity layer, even a thin layer can produce a significant increase in conductor temperature. This effect is considerably greater than that of a similar high-resistivity inclusion located farther from the cable, where its contribution to the overall heat-dissipation process is less significant. Small variations in the thickness of the peat layer around the cable can produce substantial differences in both conductor temperature and equivalent thermal resistivity. This introduces uncertainty into the thermal assessment when the exact extent of the peat layer is not well defined. The uncertainty is further increased by the absence of a direct thermal resistivity measurement within this layer. Thin high-resistivity layers located near the cable depth should therefore be carefully considered, particularly when their thermal properties and spatial extent are uncertain.

The real case scenarios highlight the difficulties and risks associated with the thermal characterisation of the seabed. Thermal resistivity measurements alone are not sufficient to fully describe the soil thermal behaviour around the cable. A careful evaluation of the stratigraphy, layer continuity, burial-depth variations, and possible high-resistivity layers where no direct measurements are available is also necessary.

For this reason, investigation locations should not be assessed independently. Comparison with adjacent locations is needed to evaluate possible layer continuity and to verify whether the selected burial depth may cause the cable to intersect unfavourable soil layers along the route. This helps reduce the risk of unidentified high-resistivity zones and local thermal hotspots. These aspects show that the interpretation of soil thermal behaviour is not only relevant for the calculation of equivalent thermal resistivity, but also for the selection of a suitable cable design solution and for route assessment. In some cases, the thermal interpretation may also support decisions on burial depth or local route adjustments.

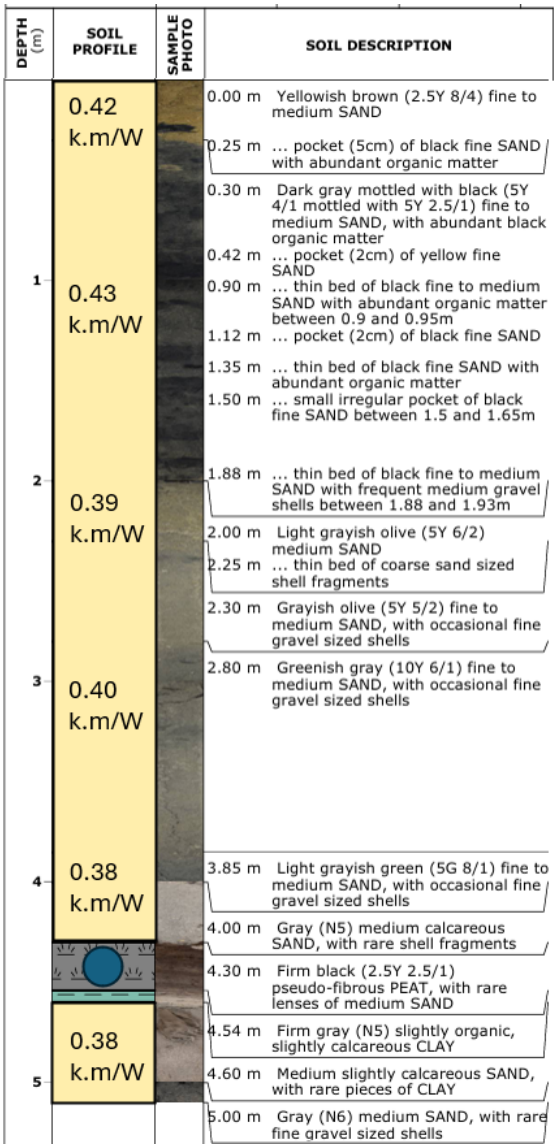


**Figure 20.** Soil stratigraphy at Location C. The recovered sample, interpreted soil layers, assigned thermal resistivity values, and cable position are shown.

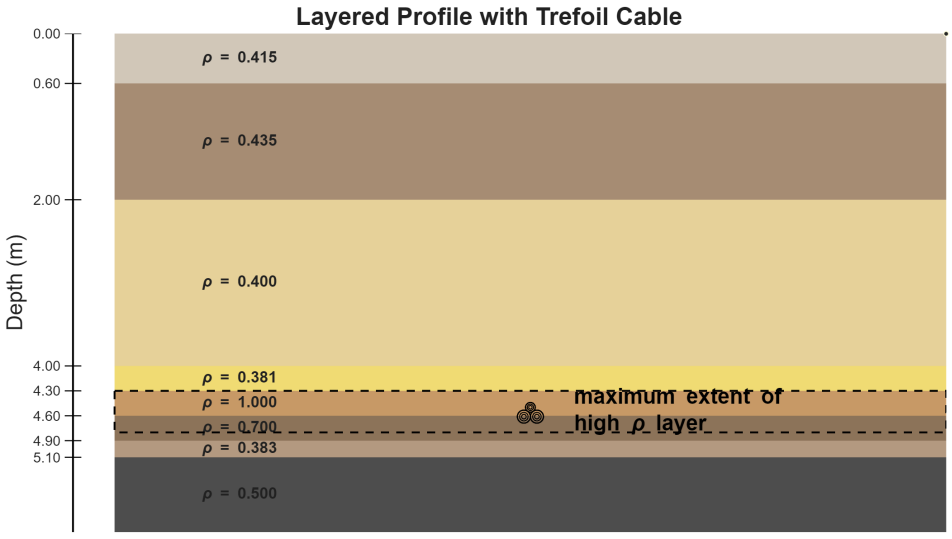


**Figure 21.** Soil stratigraphy at Location C used in the simulations.

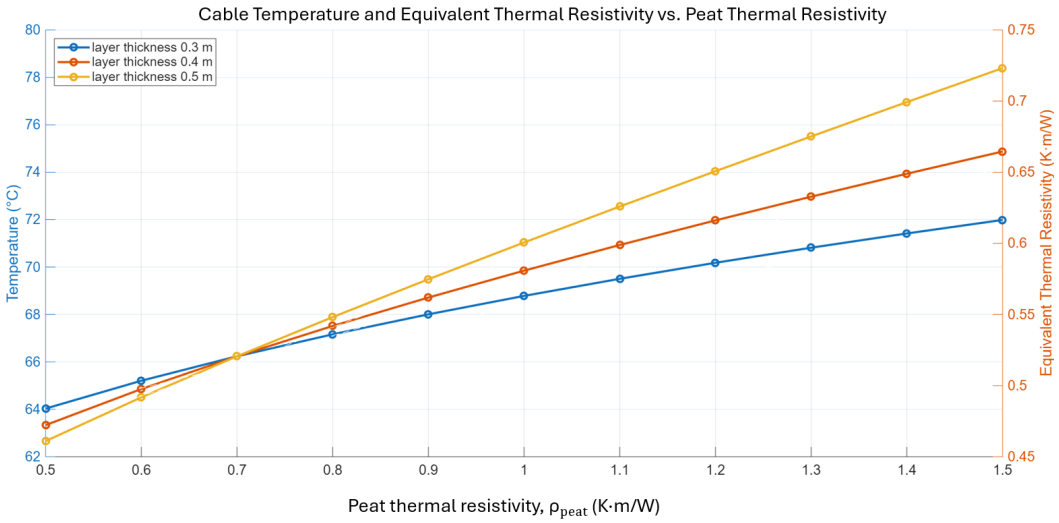


**Figure 22.** Effect of the assumed peat-layer thickness and thermal resistivity at Location C on the conductor temperature and equivalent thermal resistivity, obtained from COMSOL finite-element simulations using the soil stratigraphy shown in Figure 21.

### *6.3. Implementation in Cable Design and Route Finalisation*

The previous sections described how soil investigation data can be interpreted and converted into equivalent thermal resistivity values for ampacity calculations. In practice, these values form part of the technical input provided to cable manufacturers during the tender stage, together with other design requirements and installation conditions. Based on this information, manufacturers can prepare a preliminary cable system design that satisfies the required transmission capacity and thermal limits.

After the tender evaluation, the preferred supplier is selected by considering both technical and economic aspects. This selection is made only if the required prerequisites are fulfilled, including qualification requirements, suitable technology, production capacity, and compliance with the employer requirements. Once the supplier has been selected, the design process is further refined.

During the later project stages, more detailed studies of the cable route are performed. These may include updates to the installation route, burial depth, and local seabed conditions based on the contractor's route survey activities. At the same time, route clearance is carried out. This may include the removal of obstacles, debris, out-of-service cables, and unexploded ordnance (UXO), which refers to explosive objects that remain in the seabed from past military activities and have not detonated.

After completion of the detailed route studies and route clearance, the final cable route can be defined. The final cable design is then developed by the supplier based on the confirmed route, the installation conditions, the employer requirements, the manufacturer's design philosophy, and the expected operating conditions along the route. The supplier performs the required design verification and delivers the final detailed design to the employer.

Based on the final design, the employer performs an internal re-check of the cable ampacity along the full route. This verification considers the final cable design, the confirmed installation conditions, and possible future changes in operational conditions. The cable design proposed by the supplier is accepted only after the ampacity calculations and supporting design documentation have been reviewed. Finally, prototyping and testing are performed according to the applicable international standards and guidelines.

This process shows how the equivalent thermal resistivity assessment developed in this work fits into the wider cable design workflow. A consistent and transparent method

for deriving equivalent thermal resistivity values supports the tender process, improves comparability between supplier designs, and provides a reliable basis for later ampacity checks once the final route and cable design are defined.

## 7. Conclusions

This paper presented a methodology for deriving equivalent soil thermal resistivity values from layered offshore soil profiles for use in EHVDC cable design. The approach combines geotechnical interpretation, thermal resistivity measurements, statistical soil-type characterisation, and a conformal-mapping-based thermal solver to convert layered seabed conditions into equivalent homogeneous thermal resistivity values suitable for standard ampacity calculations.

A key finding is that the assignment of thermal resistivity values to individual soil layers cannot be based solely on available thermal measurements. Stratigraphic information obtained from CPT data and visual inspection of recovered soil samples must also be considered. For layers where direct measurements are not available, representative values derived from statistical soil-type characterisation provide a more consistent basis for interpretation. This is important because thermal resistivity can vary significantly between different soil materials, directly affecting ampacity calculations.

The developed conformal-mapping-based solver was validated against finite-element simulations and showed good agreement, confirming that it provides reliable estimates of equivalent thermal resistivity while requiring significantly less modelling effort than detailed numerical analyses.

The sensitivity analyses showed that the equivalent thermal resistivity is mainly governed by the soil conditions surrounding the cable, while far-field soil assumptions and small lateral variations generally have a limited influence. However, the analyses and real case studies demonstrated that changes in layer thickness, layer depth, and cable burial depth between investigation locations can determine whether high-resistivity materials influence the cable thermal response. Thermal resistivity measurements alone are therefore insufficient to fully characterise the seabed. Stratigraphy, layer continuity, burial-depth variations, and missing measurements in high-resistivity layers must also be considered.

Overall, this study demonstrates that equivalent thermal resistivity assessment is both a numerical calculation problem and a soil interpretation problem. A systematic and transparent derivation procedure can support robust cable design, improve comparability during tendering, and help identify locations where additional conservatism, detailed verification, or route and burial-depth adjustments may be required.

Future work should focus on improving the treatment of spatial uncertainty between investigation locations, including probabilistic approaches for layer continuity, missing thermal resistivity values, and burial-depth variability. Additional comparison with in situ thermal resistivity measurements would also help reduce uncertainty and improve confidence in equivalent thermal resistivity assessments.

**Author Contributions:** Conceptualization, F.M., I.C., F.d.V., B.S., L.C. and M.G.N.; methodology, F.M., I.C. and L.C.; software, F.M.; validation, F.M.; formal analysis, F.M.; investigation, F.M.; data curation, F.M.; writing—original draft preparation, F.M., I.C., F.d.V., B.S., L.C. and M.G.N.; writing—review and editing, F.M., I.C., F.d.V., B.S., L.C. and M.G.N.; visualization, F.M., I.C., F.d.V., B.S., L.C. and M.G.N.; supervision, F.M., I.C., F.d.V., B.S., L.C. and M.G.N. All authors have read and agreed to the published version of the manuscript.

**Funding:** This research received no external funding.

**Institutional Review Board Statement:** Not applicable.

**Informed Consent Statement:** Not applicable.

**Data Availability Statement:** The data used in this study are not publicly available due to project confidentiality restrictions.

**Acknowledgments:** The authors acknowledge TenneT TSO B.V. and the university supervisors for their support during this work.

**Conflicts of Interest:** Authors Ioannis Chatzis, Lukasz Chmura, Beate Simon, and Frank de Vries were employed by the company TenneT TSO B.V. The remaining authors declare that this research was conducted in the absence of any commercial or financial relationships that could be construed as potential conflicts of interest.

## Abbreviations

The following abbreviations are used in this manuscript:

| | |
|---|---|
| CPT | Cone Penetration Test |
| CPTU | Cone Penetration Test with pore-pressure measurement |
| EHVDC | Extra-high-voltage direct current |
| FEM | Finite element method |
| HVDC | High-voltage direct current |
| TR | Thermal resistivity |
| TSO | Transmission system operator |

## References

1. European Commission. Offshore Renewable Energy. Available online: https://energy.ec.europa.eu/topics/renewable-energy/offshore-renewable-energy_en (accessed on 14 May 2026).
2. European Commission. Member States Agree New Ambition for Expanding Offshore Renewable Energy. 2024. Available online: https://energy.ec.europa.eu/news/member-states-agree-new-ambition-expanding-offshore-renewable-energy-2024-12-18_en (accessed on 14 May 2026).
3. Callender, G.; Goddard, K.F.; Dix, J.K.; Lewin, P.L. A Flexible Model to Calculate Buried Cable Ampacity in Complex Environments. *IEEE Trans. Power Deliv.* **2022**, *37*, 2007–2015. [CrossRef]
4. Swaffield, D.; Lewin, P.; Sutton, S.J. Methods for Rating Directly Buried High Voltage Cable Circuits. *Gener. Transm. Distrib. IET* **2008**, *2*, 393–401. [CrossRef]
5. Duraisamy, N.; Gooi, H.B.; Ukil, A. Ampacity Estimation for HV Submarine Power Cables Installed in Saturated Seabed. In Proceedings of the 2018 IEEE International Conference on Power Electronics, Drives and Energy Systems (PEDES), Chennai, India, 18–21 December 2018; pp. 1–5. [CrossRef]
6. Anderson, N.L.; Croxton, N.; Hoover, R.; Sirles, P. *Geophysical Methods Commonly Employed for Geotechnical Site Characterization*; Technical Report Transportation Research Circular E-C130; Transportation Research Board of the National Academies: Washington, DC, USA, 2008.
7. Srinaiah, J.; Senthil, P.; Sarwade, D.V.; Dev, H. Applications of Geophysical Methods for Subsurface Geological and Geotechnical Assessment: An Overview. *Int. J. Innov. Sci. Res. Technol.* **2022**, *7*, 805–811. [CrossRef]
8. CIGRE Working Group 21.02. *The Calculation of the Effective External Thermal Resistance of Cables Laid in Materials Having Different Thermal Resistivities*; Technical Report ELT_098_2; CIGRE: Paris, France, 1985.
9. *IEC 60287-1-1*; Electric Cables—Calculation of the Current Rating—Part 1-1: Current Rating Equations 100% Load Factor and Calculation of Losses—General, 2006. International Electrotechnical Commission: Geneva, Switzerland, 2006.
10. CIGRE Working Group B1.62. *Recommendations for Testing DC Extruded Cable Systems for Power Transmission at a Rated Voltage Up to and Including 800 kV*; Technical Brochure 852; CIGRE: Paris, France, 2021.
11. Fabiani, D.; Montanari, G.C.; Laurent, C.; Teyssedre, G.; Morshuis, P.H.F.; Bodega, R.; Dissado, L.A. HVDC Cable Design and Space Charge Accumulation. Part 3: Effect of Temperature Gradient. *IEEE Electr. Insul. Mag.* **2008**, *24*, 5–14. [CrossRef]
12. *IEC 60287-2-1*; Electric Cables—Calculation of the Current Rating—Part 2-1: Thermal Resistance—Calculation of Thermal Resistance. International Electrotechnical Commission: Geneva, Switzerland, 2015.
13. Lunne, T.; Robertson, P.K.; Powell, J.J.M. *Cone Penetration Testing in Geotechnical Practice*; Blackie Academic & Professional: London, UK, 1997.
14. Robertson, P.K. *Guide to Cone Penetration Testing*, 7th ed.; Gregg Drilling & Testing, Inc.: Signal Hill, CA, USA, 2024.
15. *IEEE Std 442-1981*; IEEE Guide for Soil Thermal Resistivity Measurements, 1981. Institute of Electrical and Electronics Engineers: New York, NY, USA, 1981.

16. *ASTM D5334-14*; Standard Test Method for Determination of Thermal Conductivity of Soil and Soft Rock by Thermal Needle Probe Procedure. ASTM International: West Conshohocken, PA, USA, 2014.
17. FIELAX GmbH. Principle of Measurement. Available online: https://www.fielax.de/en/principle-of-measurement/ (accessed on 14 May 2026).
18. Kullback, S.; Leibler, R.A. On Information and Sufficiency. *Ann. Math. Stat.* **1951**, *22*, 79–86. [CrossRef]
19. Burnham, K.P.; Anderson, D.R. *Model Selection and Multimodel Inference: A Practical Information-Theoretic Approach*, 2nd ed.; Springer: New York, NY, USA, 2002.
20. Netherlands Enterprise Agency (RVO); Fugro. *Integrated Ground Model: IJmuiden Ver Wind Farm Zone, Sites I–IV*; Technical Report IJV_20230127_RVO_IGM_FUG 04; Integrated Ground Model Report for the IJmuiden Ver Wind Farm Zone; Netherlands Enterprise Agency (RVO): The Hague, The Netherlands, 2023.
21. Rijsdijk, K.F.; Passchier, S.; Weerts, H.J.T.; Laban, C.; van Leeuwen, R.J.W.; Ebbing, J.H.J. Revised Upper Cenozoic Stratigraphy of the Dutch Sector of the North Sea Basin: Towards an Integrated Lithostratigraphic, Seismostratigraphic and Allostratigraphic Approach. *Neth. J. Geosci.* **2005**, *84*, 129–146. [CrossRef]

**Disclaimer/Publisher's Note:** The statements, opinions and data contained in all publications are solely those of the individual author(s) and contributor(s) and not of MDPI and/or the editor(s). MDPI and/or the editor(s) disclaim responsibility for any injury to people or property resulting from any ideas, methods, instructions or products referred to in the content.